© 2015. Published by The Company of Biologists Ltd | Journal of Cell Science (2015) 128, 3466-3477 doi:10.1242/jcs.173013

RESEARCH ARTICLE

The lysine demethylase LSD1 is required for nuclear envelope formation at the end of mitosis

Allana Schooley, Daniel Moreno-Andrés, Paola De Magistris, Benjamin Vollmer* and Wolfram Antonin‡

ABSTRACT

The metazoan nucleus breaks down and reassembles during each cell division. Upon mitotic exit, the successful reestablishment of an interphase nucleus requires the coordinated reorganization of chromatin and formation of a functional nuclear envelope. Here, we report that the histone demethylase LSD1 (also known as KDM1A) plays a crucial role in nuclear assembly at the end of mitosis. Downregulation of LSD1 in cells extends telophase and impairs nuclear pore complex assembly. *In vitro*, LSD1 demethylase activity is required for the recruitment of MEL28 (also known as ELYS and AHCTF1) and nuclear envelope precursor vesicles to chromatin, crucial steps in nuclear reassembly. Accordingly, the formation of a closed nuclear envelope and nuclear pore complex assembly are impaired upon depletion of LSD1 or inhibition of its activity. Our results identify histone demethylation by LSD1 as a new regulatory mechanism linking the chromatin state and nuclear envelope formation at the end of mitosis.

KEY WORDS: Nuclear envelope formation, Nuclear pore complex, Mitotic exit, Lysine (K)-specific demethylase 1A, KDM1A, Histone modification, MEL28, ELYS, POM121, NDC1

INTRODUCTION

The nuclear genome is organized and maintained within the two membranes of the nuclear envelope. The envelope itself is a compartment of the endoplasmic reticulum (ER) and the outer nuclear membrane is continuous with the ER network. The inner nuclear membrane contains a unique set of integral membrane proteins that connect to chromatin and the nuclear lamina. The exchange of molecules between the cytoplasm and the nucleoplasm is mediated by nuclear pore complexes (NPCs), macromolecular protein assemblies that are found at points of fusion between the inner and outer membranes of the nuclear envelope. In metazoa, the nuclear envelope breaks down during mitosis in order to facilitate the capture of highly condensed chromosomes and their segregation by the spindle apparatus. The complex architecture of the interphasic nucleus must therefore be reestablished upon mitotic exit when the nuclear envelope and pore complexes reassemble on the decondensing chromatin (for reviews see Güttinger et al., 2009; Schooley et al., 2012).

Phosphorylation cascades regulate the structural changes to nuclear organization that occur during mitosis, including massive chromatin condensation and nuclear envelope disassembly. At the onset of mitosis, the phosphorylation of lamins (Heald and McKeon, 1990; Peter et al., 1990) and inner nuclear membrane proteins (Foisner and Gerace, 1993; Pyrpasopoulou et al., 1996) initiates the disassembly of the nuclear envelope. The reestablishment of the interphase nucleus at the end of mitosis is coordinated by the reversal of mitotic phosphorylation events due to the inactivation of mitotic kinases and the activation of phosphatases (Wurzenberger and Gerlich, 2011). Dephosphorylation of lamins enables the reassembly of the nuclear lamina (Thompson et al., 1997). Meanwhile dephosphorylation of inner nuclear membrane proteins increases their affinity for chromatin and initiates nuclear membrane recruitment (Pfaller et al., 1991; Ito et al., 2007) and nuclear envelope formation.

Upon nuclear disassembly, the nuclear membranes are absorbed in the mitotic ER and it is currently unclear whether they maintain their identity as a distinct subcompartment within the network during mitosis. Experiments in *Xenopus laevis* egg extracts, which have been used extensively to study nuclear envelope and NPC assembly in cell-free systems (Gant and Wilson, 1997), suggest that indeed they do maintain their identity. The ER derived from egg extract preparations gives rise to distinct vesicle populations that possess different capacities to support nuclear envelope formation. One such population is enriched for the transmembrane nucleoporins POM121 and NDC1, has a high affinity for chromatin, and is part of the initial wave of nuclear membrane recruitment to chromatin during cell-free nuclear assembly (Antonin et al., 2005; Mansfeld et al., 2006). A second vesicle population has a lower affinity for chromatin, is recruited relatively late during nuclear assembly, and is enriched for a third transmembrane nucleoporin, GP210 (also known as NUP210). These distinct vesicle types can also be biochemically separated from a third vesicle pool enriched for typical ER-membrane proteins, which are not strictly essential for nuclear assembly. The physical and functional separation of nuclear membrane vesicle populations implies that there is microscale partitioning of different membrane domains in the mitotic ER. At the end of mitosis, nuclear membranes segregate from the bulk ER and enclose the decondensing chromatin to form a new nuclear envelope. Chromatin binding by integral inner nuclear membrane proteins is thought to be a crucial determinant in this process (Ulbert et al., 2006; Anderson et al., 2009).

Concomitant with the formation of the nuclear envelope and thus the establishment of a diffusion barrier between the cytoplasm and the nuclear interior, NPCs re-assemble to ensure its transport competence (Bodoor et al., 1999; Daigle et al., 2001). Post-mitotic NPC assembly is initiated by the recruitment of a subset of nucleoporins to chromatin and is particularly well characterized due to the faithful reconstitution of these events in *Xenopus* egg extracts. The chromatin-binding nucleoporin MEL28 (also known as ELYS and AHCTF1) initiates NPC

Friedrich Miescher Laboratory of the Max Planck Society, Spemannstraße 39, Tübingen 72076, Germany.
*Present address: Oxford Particle Imaging Centre, Division of Structural Biology, Wellcome Trust Centre for Human Genetics, University of Oxford, Oxford OX3 7BN, UK.

‡Author for correspondence (wolfram.antonin@tuebingen.mpg.de)

Received 10 April 2015; Accepted 27 July 2015

Journal of Cell Science

Journal of Cell Science (2015) 128, 3466-3477 doi:10.1242/jcs.173013

assembly by recruiting the Nup107–Nup160 complex, a major structural component of the NPC (Harel et al., 2003; Walther et al., 2003b; Rasala et al., 2006, 2008; Franz et al., 2007; Gillespie et al., 2007; Rotem et al., 2009). Membranes are next connected to the assembling NPC by interactions between the transmembrane nucleoporin POM121 and the Nup107–Nup160 complex (Antonin et al., 2005; Mitchell et al., 2010; Yavuz et al., 2010). NDC1 is also likely to be involved at this step (Mansfeld et al., 2006; Stavru et al., 2006) but its function is less defined. Components of the second major structural subunit of the NPC, the Nup93 complex, subsequently assemble stepwise from the membrane building laterally towards the centre of the NPC (Dultz et al., 2008; Sachdev et al., 2012; Vollmer et al., 2012), which allows for the recruitment of the central channel components, the FG-nucleoporins. The final steps of NPC assembly are the addition of peripheral nucleoporins, which form extensions to the cytoplasmic and nucleoplasmic sides of the pore (Bodoor et al., 1999; Hase and Cordes, 2003; Dultz et al., 2008). The small GTPase ran spatially regulates NPC reassembly by promoting the release of transport receptor bound proteins, such as MEL28 (Franz et al., 2007; Rotem et al., 2009), at post-mitotic chromatin (Walther et al., 2003a). Several nucleoporins are also hyper-phosphorylated during mitosis (Laurell et al., 2011) but the extent to which their dephosphorylation regulates post-mitotic NPC formation is currently not clear.

Although the crucial events of post-mitotic nuclear envelope assembly occur on decondensing chromatin, the regulatory mechanisms that coordinate envelope assembly and the chromatin state at that time are not well understood. Here, we identify dynamic demethylation of histone H3 by the Lysine (K) Specific Demethylase, LSD1 (also known as KDM1A), as a new mechanism coordinating the recruitment and assembly of nuclear envelope and NPC components on post-mitotic chromatin. We report that the loss of LSD1 demethylase activity blocks nuclear envelope and pore complex formation *in vitro*, through impaired recruitment of MEL28, and POM121- and NDC1-containing membrane vesicles. We find that downregulation of LSD1 in human cells elongates telophase and results in ectopic NPC assembly outside of the nuclear envelope. Our data imply that LSD1-dependent demethylation of histones is a requirement for proper nuclear assembly at the end of mitosis.

RESULTS

LSD1 demethylase activity is required for cell-free nuclear assembly

In an effort to identify regulatory landmarks of nuclear envelope reassembly at the end of mitosis we screened various classes of chemical inhibitors for their ability to block nuclear assembly *in vitro*. Cell-free nuclear formation can be faithfully recapitulated on a sperm chromatin template using the cytosolic and membrane fractions of *Xenopus laevis* egg extracts induced to mimic the late mitotic state (for a review, see Gant and Wilson, 1997). After initial DNA decondensation, a nuclear envelope forms around the chromatin, which continues to decondense and reorganize, giving rise to a functionally competent nucleus. A closed nuclear envelope can be visualized by the smooth nuclear rim incorporation of the fluorescent lipophilic membrane dye 1,1′-Dioctadecyl-3,3,3′,3′-tetramethylindocarbocyanine perchlorate (DiIC18) (Fig. 1, untreated). NPCs are integrated in the newly formed envelope and can be observed by immunolabelling with mAB414, an antibody that recognizes a subset of FG-repeat-containing nucleoporins (Davis and Blobel, 1986). We identified a group of inhibitors [*N*-methyl-*N*-propargylbenzylamine (pargyline), *trans*-2-phenylcyclopropylamine (2-PCPA), and the 2-PCPA derivative trans-2-(2-benzyloxy-3,5-difluorophenyl)cyclopropylamine hydrochloride (S2101)] targeting the histone lysine demethylase LSD1 that severely impairs nuclear envelope and NPC assembly (Fig. 1).

In order to determine whether LSD1 specifically plays a role in nuclear assembly it was immuno-depleted from *Xenopus* egg extract cytosol using a polyclonal antibody generated against full-length *Xenopus* LSD1 that recognizes both the *Xenopus* and human protein (supplementary material Fig. S1). LSD1 was efficiently removed from the egg cytosol, whereas the levels of other proteins, including the nucleoporins Nup107, Nup62 and MEL28, the nuclear GTPase ran, which is important for nuclear transport, and CoREST (also known as RCOR1), which functions as an LSD1 cofactor in H3K4 demethylation (Shi et al., 2005), were unaffected (Fig. 2A). LSD1 depletion rendered the extracts incompetent for nuclear envelope and NPC assembly (Fig. 2B,C). Addition of purified recombinant *Xenopus* LSD1 rescued the formation of a closed nuclear envelope with integrated NPCs, validating the specificity of the depletion phenotype and confirming the requirement for LSD1 in nuclear assembly. We designed a demethylase-deficient version of LSD1 by

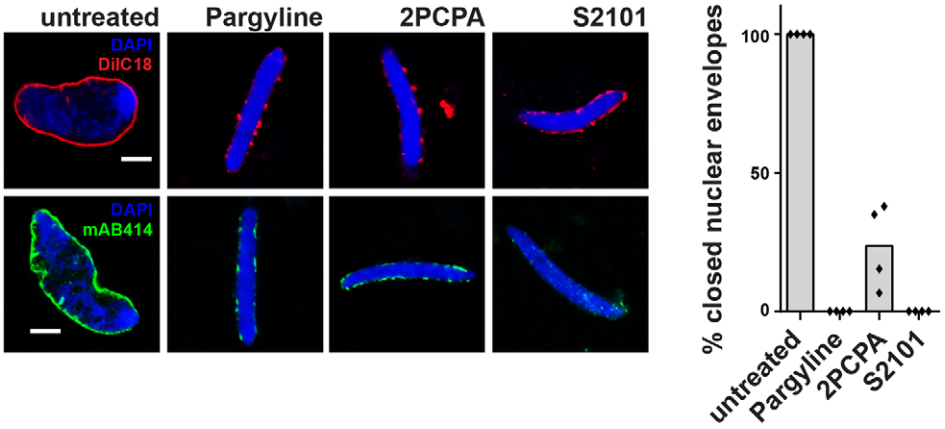

Fig. 1. LSD1 inhibitors block cell-free nuclear assembly. Nuclei assembled on sperm chromatin in *Xenopus* egg extracts for 120 min were fixed and analyzed by confocal microscopy. Where indicated 5 mM pargyline, 2.5 mM 2PCPA or 0.25 mM S2101 was added to assembly reactions at *t*=0. Membranes were pre-labelled with DiIC18 (upper panel, red in overlay), NPCs were immuno-labelled following fixation using mAB414 (lower panel, green), and chromatin was stained with DAPI (blue in overlays). Scale bars: 5 µm. In each experiment, 100 randomly chosen chromatin substrates were scored. The mean percentage of nuclei with closed nuclear envelopes from four independent experiments is shown. Data points from individual experiments are indicated.

Journal of Cell Science (2015) 128, 3466-3477 doi:10.1242/jcs.173013

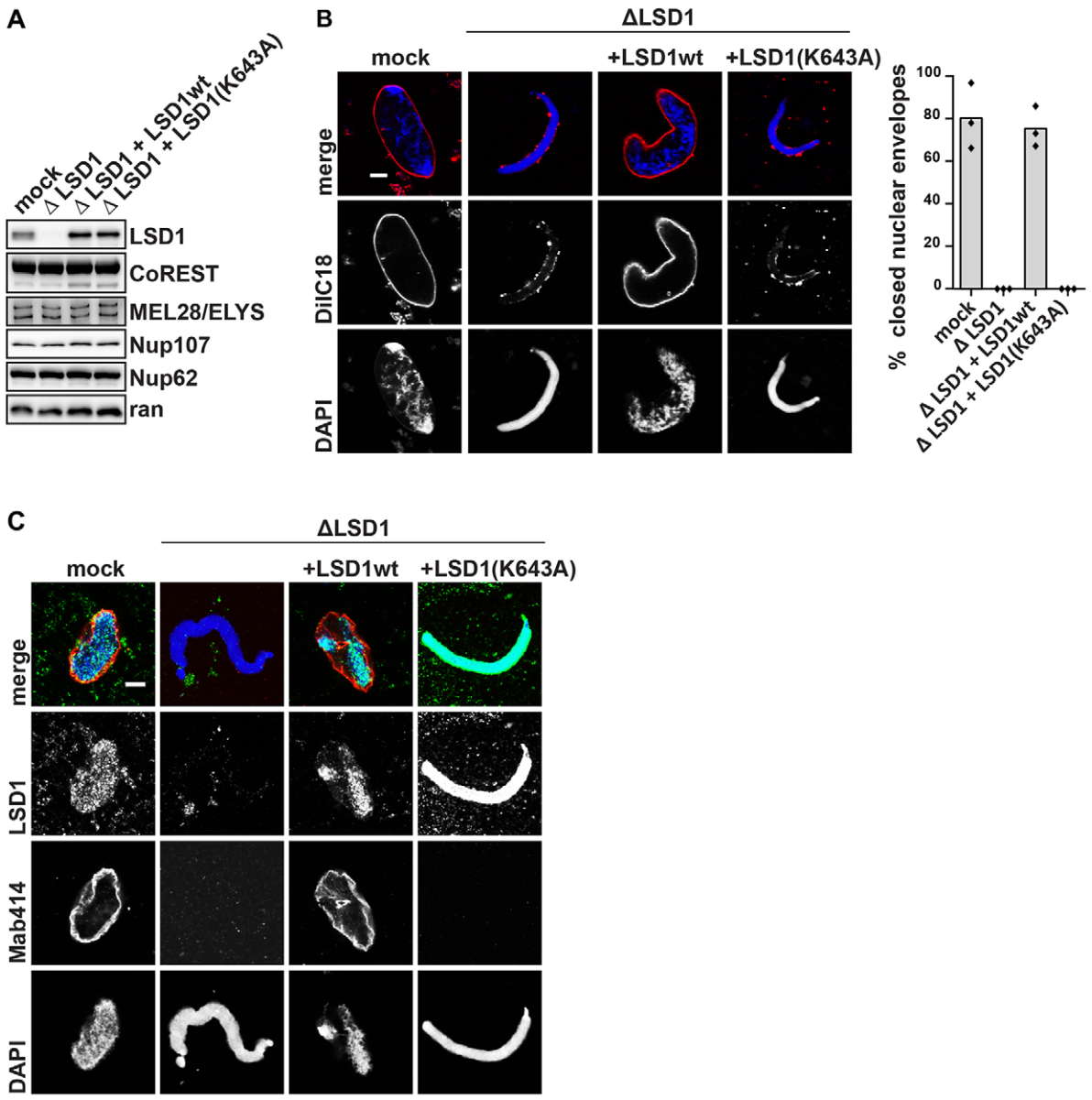

Fig. 2. Cell-free nuclear assembly requires the demethylase activity of LSD1. (A) Western blot analysis of mock-depleted, LSD1-depleted (ΔLSD1), and LSD1-depleted *Xenopus* egg extracts supplemented with either recombinant wild-type LSD1 (LSD1wt) or the catalytically inactive LSD1(K643A) mutant. (B) Confocal microscopy images of fixed nuclei assembled for 120 min in the indicated extract conditions. Membranes were pre-labelled with DiIC18 (red in overlay) and chromatin was stained with DAPI (blue in overlay). The mean percentage of closed nuclear envelopes for 100 randomly chosen chromatin substrates in each of three independent experiments is shown. Data points from individual experiments are indicated. (C) Nuclei assembled for 120 min in the indicated extract conditions were fixed and analyzed for the presence of immunolabelled LSD1 (green in overlay) and NPCs (mAB414, red in overlay) on the chromatin (DAPI, blue in overlay) by confocal microscopy. Scale bars: 5 µm.

mutating a lysine residue in the FAD-binding pocket, based on structural and functional studies of the human homologue (Stavropoulos et al., 2006). This catalytically inactive LSD1 mutant [a lysine residue exchanged to an alanine residue in position 643, LSD1(K643A)] failed to rescue the nuclear assembly defect (Fig. 2B,C), indicating that the demethylase activity of LSD1 is crucial for nuclear envelope and NPC assembly.

Loss of LSD1 in human cells extends telophase and promotes the formation of annulate lamellae

We performed immunofluorescence experiments in HeLa cells and found that LSD1 localized to the nucleus during interphase but was largely excluded from chromatin during mitosis (supplementary material Fig. S2). It could first be seen re-associating with chromatin early in telophase coincident with NPC formation, which was detected by mAB414 staining (supplementary material Fig. S2A,B), and prior to abscission, which was visualized by the loss of midbody-associated α-tubulin between the segregated chromatin masses (supplementary material Fig. S2C) (Guizetti et al., 2011). To assay the importance of LSD1 during mitotic exit in cells, we employed RNA interference (RNAi) and followed mitotic events by live-cell imaging. LSD1 was efficiently depleted by small interfering RNA (siRNA) for up to 72 h in HeLa cells stably expressing histone H2B fused to a mCherry reporter (Fig. 3A; supplementary material Fig. S3A). Cells were imaged over ∼20 h by time-lapse fluorescence microscopy and chromatin features were

Journal of Cell Science (2015) 128, 3466-3477 doi:10.1242/jcs.173013

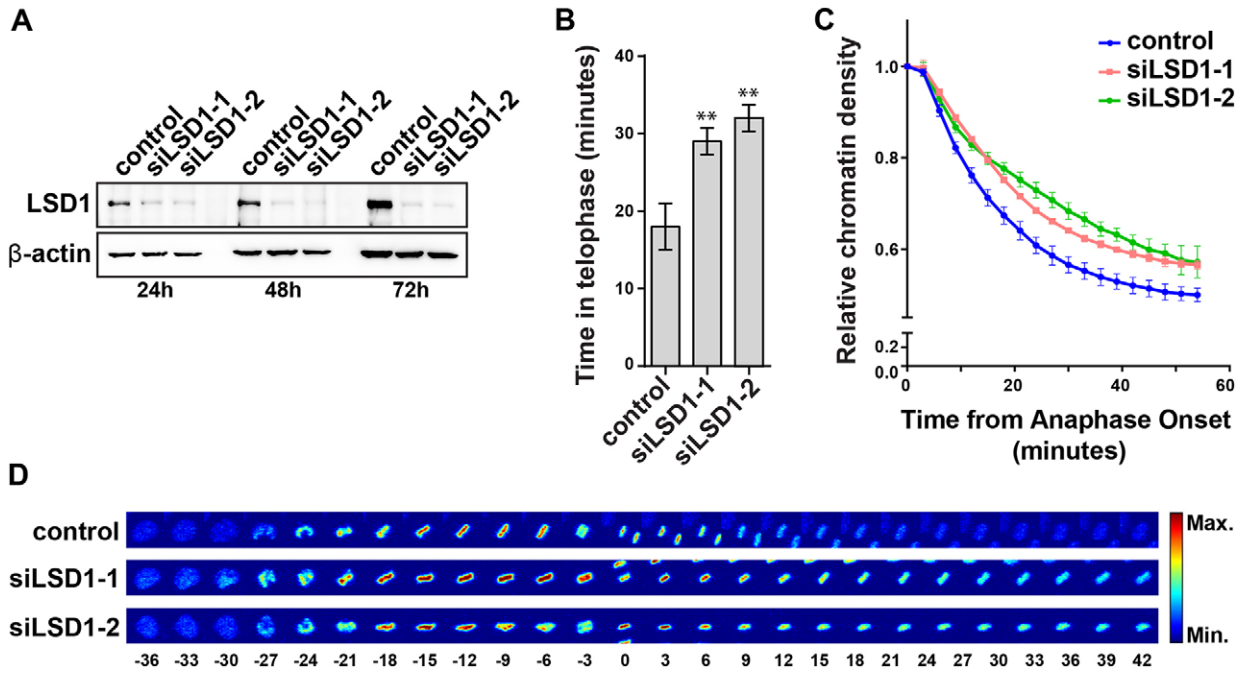

Fig. 3. LSD1 is required for the timely establishment of interphasic chromatin after mitosis in human cells. (A) Western blot analysis of whole-cell lysates from HeLa cells stably expressing H2B–mCherry and transfected with 20 nM control, siLSD1-1 or siLSD1-2 siRNA oligonucleotides as indicated. Lysates were harvested at 24, 48 and 72 h post-transfection. (B) HeLa cells stably expressing H2B–mCherry and transfected with 20 nM siRNA as indicated were subjected to time-lapse microscopy starting 30 h after transfection. Mitotic events were analyzed with CellCognition. The mean of the median time spent in telophase is plotted for more than 100 mitotic events per condition in three independent experiments. Error bars represent s.d. $^{**}P<0.01$ (Student's *t*-test). (C) The average fluorescence intensity of the H2B–mCherry signal was extracted from the CellCognition data acquired in B as an indication of chromatin density. The density was normalized to the first anaphase frame in individual mitotic tracks and the mean relative density for more than 100 mitotic events per condition from three independent experiments is plotted over time. Error bars represent s.d. (D) HeLa cells stably expressing H2B–mCherry and transfected with 20 nM siRNA were subjected to time-lapse microscopy starting at 30 h after transfection. Maximum intensity projections of the mCherry signal from five optical *z* sections are represented as heat maps. Mitotic track positions are normalized to the first anaphase frame.

annotated and tracked during mitotic events using the image analysis software CellCognition (Schmitz and Gerlich, 2009; Held et al., 2010). Based on the morphological annotation of chromatin, LSD1-depleted cells displayed a significant extension in the length of telophase (Fig. 3B). In the absence of LSD1, cells maintained condensed telophasic chromatin for 10–15 min beyond control cells, which spent an average of 18 min in telophase. Accordingly, the progressive decrease in chromatin density that occurs upon mitotic exit, based on the average fluorescence intensity of the H2B–mCherry signal, was delayed and incomplete in LSD1-depleted cells compared to controls (Fig. 3C). This extended duration of chromatin compaction following chromosome segregation could be clearly visualized in individual mitotic tracks (Fig. 3D). Although one LSD1-targeting siRNA significantly extended the duration of metaphase, the timing of other cell cycle stages was not affected by LSD1 depletion (supplementary material Fig. S3B,G) and a longer metaphase was not a prerequisite for extended chromatin compaction after anaphase (see, for example, Fig. 3D). In order to confirm that mitotic exit is delayed in the absence of LSD1, mitotic spindle dynamics were tracked in live cells stably expressing EGFP-tagged α-tubulin and mCherry–H2B. In addition to prolonged telophasic chromatin features (supplementary material Fig. S3E,F), LSD1-depleted cells maintained midbody-associated tubulin for an average of 15–30 min longer than controls, indicating that abscission, the final step in cytokinesis, is delayed (supplementary material Fig. S3I). Taken together, these data suggest that the role of LSD1 during mitosis is specific to the events occurring in telophase. Consistent with this, addition of the LSD1-targeting inhibitors 2-PCPA and S2101 to HeLa cells similarly prolonged telophase (supplementary material Fig. S4A,B).

In addition to extended telophase, the average nuclear volume in unsynchronized populations of LSD1-knockdown cells was significantly reduced compared to control populations (Fig. 4A; supplementary material Fig. S3C). This observation suggests that LSD1 depletion has a lasting effect on chromatin compaction during interphase. In order to further investigate the impact of LSD1 knockdown on nuclear architecture in interphasic cells, we employed immunofluorescent labelling of various nuclear envelope and NPC proteins. Labelling with mAB414 revealed that in addition to NPCs in the nuclear envelope, LSD1-depleted cells (Fig. 4B) or cells treated with chemical inhibitors of LSD1 (supplementary material Fig. S4C) possessed significant cytoplasmic staining for NPCs indicative of annulate lamellae. These arrays of NPCs inserted into membrane stacks of the endoplasmic reticulum (Kessel, 1992) have been found to form when post-mitotic NPC assembly is impaired (Franz et al., 2007). We counted NPCs, based on the mAB414 signal, and found a reduction in their total number at the nuclear envelope when LSD1 was depleted, although NPC density was unaffected (Fig. 4C,D).

Despite the reduction in nuclear volume and the number of NPCs at the nuclear envelope, LSD1-depleted cells were not defective in nuclear lamina assembly, as shown by the smooth rim staining of lamins A and B (Fig. 4E). Similarly, the inner nuclear envelope proteins lamin B receptor (LBR) and emerin did not seem to be affected by LSD1 knockdown and were found at the nuclear envelope. The nucleoporins Nup62, of the central channel, Nup153, from the nucleoplasmic NPC face, and Nup88, from the cytoplasmic face of the NPC, were all found at the nuclear rim in LSD1-depleted cells. Furthermore, MEL28, required for the initial

Journal of Cell Science (2015) 128, 3466-3477 doi:10.1242/jcs.173013

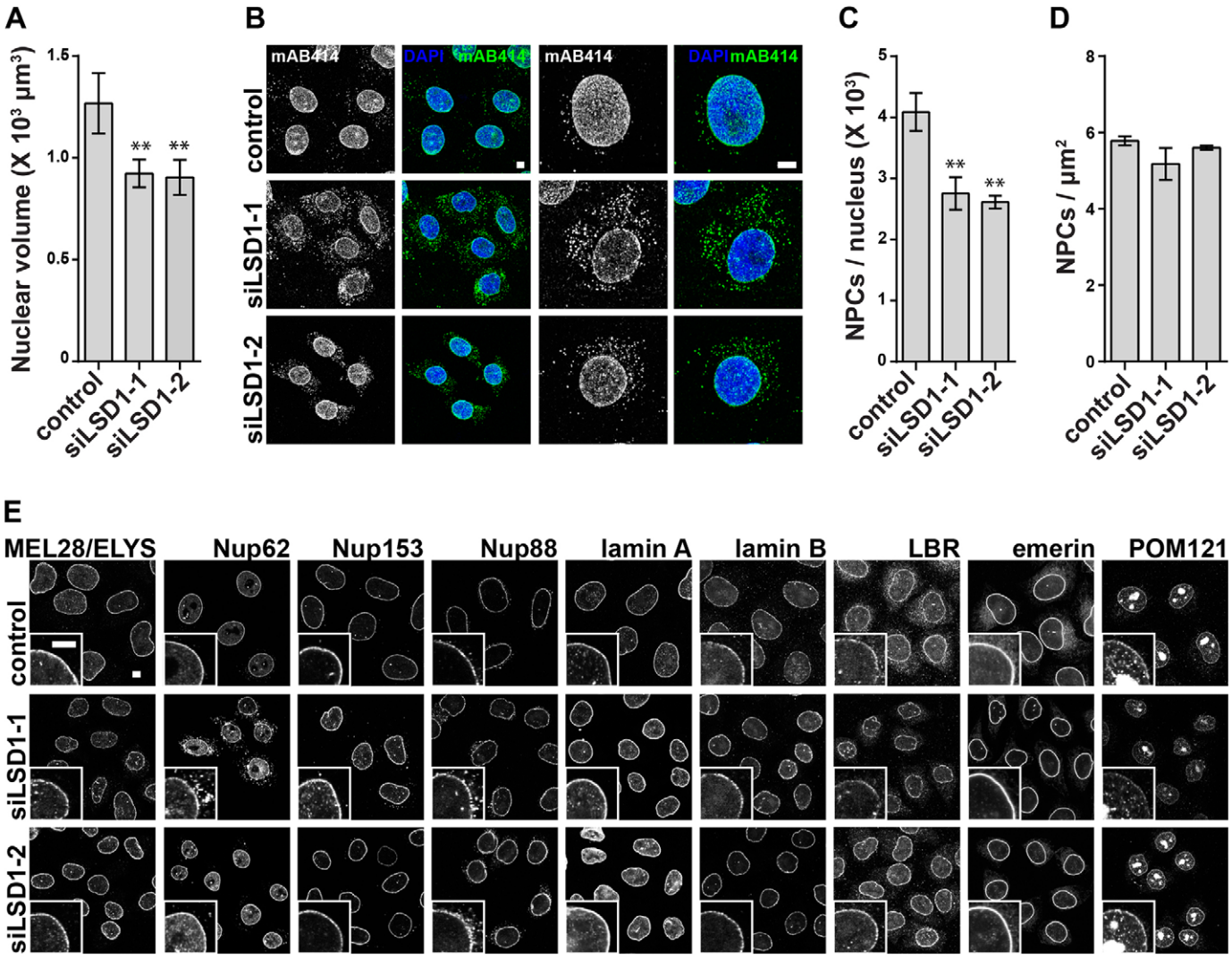

Fig. 4. Loss of LSD1 in human cells affects nuclear volume and NPC assembly. (A) Quantification of nuclear volume based on DAPI staining in HeLa cells transfected with 20 nM control, siLSD1-1 or siLSD1-2 siRNA oligonucleotides and fixed at 48 h post-transfection. The average nuclear volume from more than 80 nuclei per condition in three independent experiments is plotted. Error bars represent s.d. $^{**}P<0.01$ (Student's *t*-test). (B) HeLa cells transfected with 20 nM control, siLSD1-1 or siLSD1-2 siRNA oligonucleotides were fixed at 48 h post-transfection and processed for immunofluorescence. NPCs were immunolabelled using mAB414 (green in overlay) and DNA was stained with DAPI (blue). Maximum intensity projections are shown. (C) Quantification of mAB414-labelled NPCs in HeLa cells transfected with 20 nM control, siLSD1-1 or siLSD1-2 siRNA oligonucleotides and fixed at 48 h post-transfection. The number of NPCs over a specified surface area was counted and was used to calculate the total number per nucleus based on the nuclear volume. The mean number of NPCs per nucleus for 10 nuclei per condition in three independent experiments is plotted. Error bars represent s.d. $^{**}P<0.01$ (Student's *t*-test). (D) Quantification of NPC density in HeLa cells transfected with 20 nM control, siLSD1-1 or siLSD1-2 siRNA oligonucleotides and fixed at 48 h post-transfection. The average number of mAB414-labelled NPCs over a specified surface area was counted and the mean NPC density for 10 nuclei per condition in three independent experiments is plotted. Error bars represent s.d. (E) HeLa cells transfected with 20 nM control, siLSD1-1 or siLSD1-2 siRNA oligonucleotides were fixed at 48 h post-transfection and processed for immunofluorescence. Nuclear envelope proteins were immunolabelled as indicated and representative images are shown. Insets provide a higher magnification view. Scale bars: 5 µm.

seeding of NPC assembly on post-mitotic chromatin, and POM121, a transmembrane nucleoporin, could also be detected at the nuclear envelopes of LSD1-depleted nuclei.

Taken together, these data suggest that at the end of mitosis LSD1 is required to reestablish interphasic nuclear architecture that is conducive to nuclear expansion and NPC assembly.

LSD1 is not essential for chromatin decondensation

Nuclear reformation at the end of mitosis involves the almost simultaneous decondensation of highly compacted mitotic chromatin and assembly of a closed NPC-containing nuclear envelope (Schooley et al., 2012). Although difficult to functionally discern in a cellular context, these two integral mitotic exit processes can be biochemically separated *in vitro*. Given the apparent compaction of chromatin in both cell-free nuclear assemblies (Fig. 1A and Fig. 2B) and in HeLa cells (Fig. 3C,D) when LSD1 function was impaired, we wondered whether LSD1 had a direct role in chromatin decondensation.

The initial decondensation of sperm chromatin, the DNA template employed in our cell-free nuclear assembly assays (Figs 1 and 2), in *Xenopus* egg extracts occurs because of the exchange of sperm-specific protamines by the maternal histones H3 and H4 (Philpott and Leno, 1992). We tested whether this specialized decondensation event requires LSD1 by incubating

Journal of Cell Science (2015) 128, 3466-3477 doi:10.1242/jcs.173013

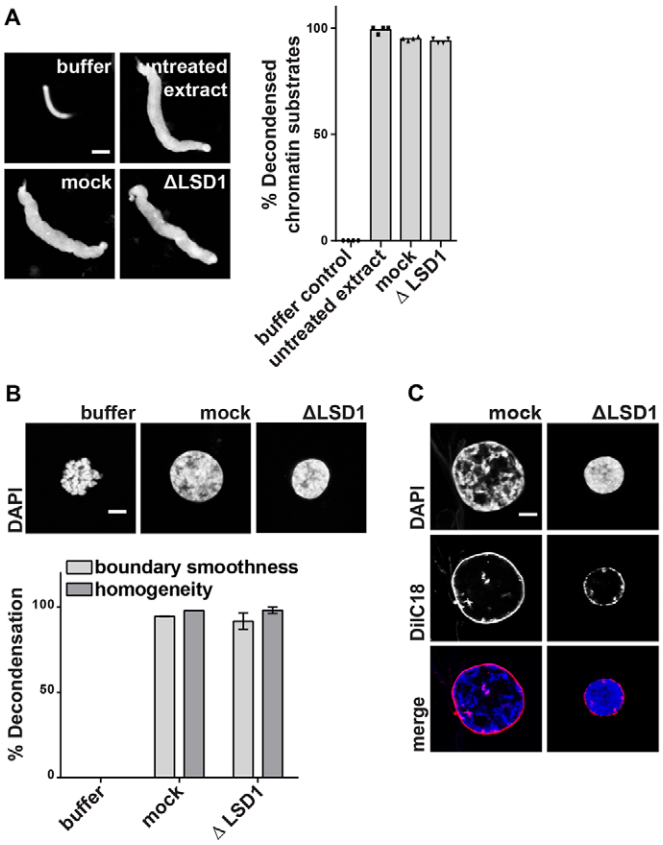

Fig. 5. LSD1 is not required for the membrane-independent decondensation of chromatin *in vitro*. (A) *Xenopus laevis* sperm chromatin heads were incubated in *Xenopus* egg extracts for 10 min, fixed and analysed by confocal microscopy. Chromatin was stained with DAPI. The mean percentage of decondensed chromatin substrates for 100 randomly chosen templates in each of four independent experiments is shown. Data points from individual experiments are indicated. (B) Mitotic chromatin clusters from HeLa cells were incubated with buffer, or mock or LSD1-depleted *Xenopus* egg extracts in the absence of added membranes. After 120 min, samples were fixed, stained with DAPI and analysed by confocal microscopy. The smoothness of the chromatin boundary (light grey) and the homogeneity of DAPI staining (dark grey) were analysed as described previously (Magalska et al., 2014). The mean percentage decondensation is plotted for 10 chromatin substrates per condition in each of three independent experiments. Error bars represent s.d. (C) Mitotic chromatin clusters from HeLa cells were incubated in mock or LSD1-depleted egg extracts in the presence of DiIC18-labelled membranes (red in overlay). Samples were fixed after 120 min, stained with DAPI (blue in overlay), and analysed by confocal microscopy. Scale bars: 5 µm.

sperm chromatin in egg extracts lacking membranes and an energy-regenerating system for 10 min. Under these conditions, histone exchange occurs and results in sperm chromatin decondensation (Fig. 5A, compare buffer to untreated extract) but nuclear assembly cannot proceed. Depletion of LSD1 did not affect sperm chromatin decondensation (Fig. 5A). Thus, the block in cell-free nuclear assembly in the absence of LSD1 activity (Figs 1 and 2) is not due to a defect in sperm DNA de-compaction.

Sperm DNA decondensation is mechanistically distinct from the decondensation of highly compacted chromatin at the end of mitosis, and we have recently established a cell-free assay to specifically analyze the latter process (Magalska et al., 2014). To this end, we examined changes to the topology of mitotic chromatin clusters isolated from HeLa cells when incubated with *Xenopus* egg extracts. In this modified version of the nuclear assembly assay, the highly condensed mitotic chromatin has been found to progressively decondense in a way that is morphologically analogous to the chromatin of cells exiting mitosis. These structural changes can be quantified based on the smoothness of the chromatin boundary and the homogeneity of DAPI staining, both increasing over time as chromatin decondenses. In the absence of membranes, depletion of LSD1 from the egg extracts had an apparently modest effect on chromatin decondensation, which was not quantifiably different based on the parameters described (Fig. 5B).

In the presence of membranes, mitotic chromatin clusters not only decondense but also support the formation of a closed nuclear envelope containing NPCs that are competent for nuclear import (Magalska et al., 2014). Accordingly, the addition of membranes to the extracts results in larger nuclei that accommodate further chromatin decondensation (Philpott et al., 1991; Wright, 1999) also known as secondary decondensation or nuclear swelling (Fig. 5C; supplementary material Fig. S4D, mock and untreated). However, when LSD1 activity was blocked by the addition of chemical inhibitors or its specific immuno-depletion, minimal membrane recruitment occurred and chromatin did not undergo any additional decondensation. Consistent with the nuclear assembly assay on sperm chromatin (Figs 1 and 2), blocking LSD1 activity impaired nuclear envelope formation on the HeLa chromatin substrate. These data suggest that LSD1 is not required for chromatin decondensation, at least the steps that occur *in vitro* in the absence of a closed nuclear envelope, but rather to render post-mitotic chromatin competent for the recruitment and assembly of nuclear envelope components.

LSD1 demethylase activity mediates the recruitment of nuclear envelope membranes and MEL28 to chromatin *in vitro*

To confirm that LSD1 plays a role in the recruitment of nuclear envelope membranes to chromatin we employed DNA-coated magnetic beads (Heald et al., 1996). DNA was chromatinized by incubation with *Xenopus* egg extract cytosol and incubated with the same membrane fractions as used in cell-free nuclear assembly reactions. Chromatinization resulted in the appearance of chromatin-binding proteins, including Ku70 (also known as XRCC6) and LSD1 (Fig. 6A), on the DNA beads. The membranes isolated from egg extracts are a mixture of different nuclear envelope precursor and ER vesicles. These include the early chromatin-binding fraction containing POM121 and NDC1, the late chromatin-binding fraction containing GP210, and a bulk ER vesicle population containing, among many other proteins, reticulon 4 (RTN4) and calnexin. Each of these membrane proteins was recruited to DNA beads chromatinized in mock-treated cytosol. However, when DNA was chromatinized in LSD1-depleted cytosol, we observed a significant reduction in the recruitment of POM121- and NDC1-containing vesicles (to 26% or 41%, respectively, Fig. 6B). The recruitment of both GP210 and ER-marker-containing vesicles (RTN4 and calnexin) was unaffected by LSD1 depletion, suggesting that membrane recruitment was not generally affected. Addition of recombinant wild-type LSD1 but not the demethylase deficient K643A mutant to LSD1-depleted extracts rescued the recruitment of POM121 and NDC1. Importantly, binding of MEL28, which is required for initiation of NPC assembly on the decondensing chromatin, was also reduced upon LSD1 depletion (to 50%) and rescued by the recombinant wild-type protein. The levels of dimethylated H3K4 were elevated by more than twofold upon LSD1 depletion or addback of the catalytically dead K643A mutant, validating H3K4me2 as an LSD1 substrate in

Journal of Cell Science (2015) 128, 3466-3477 doi:10.1242/jcs.173013

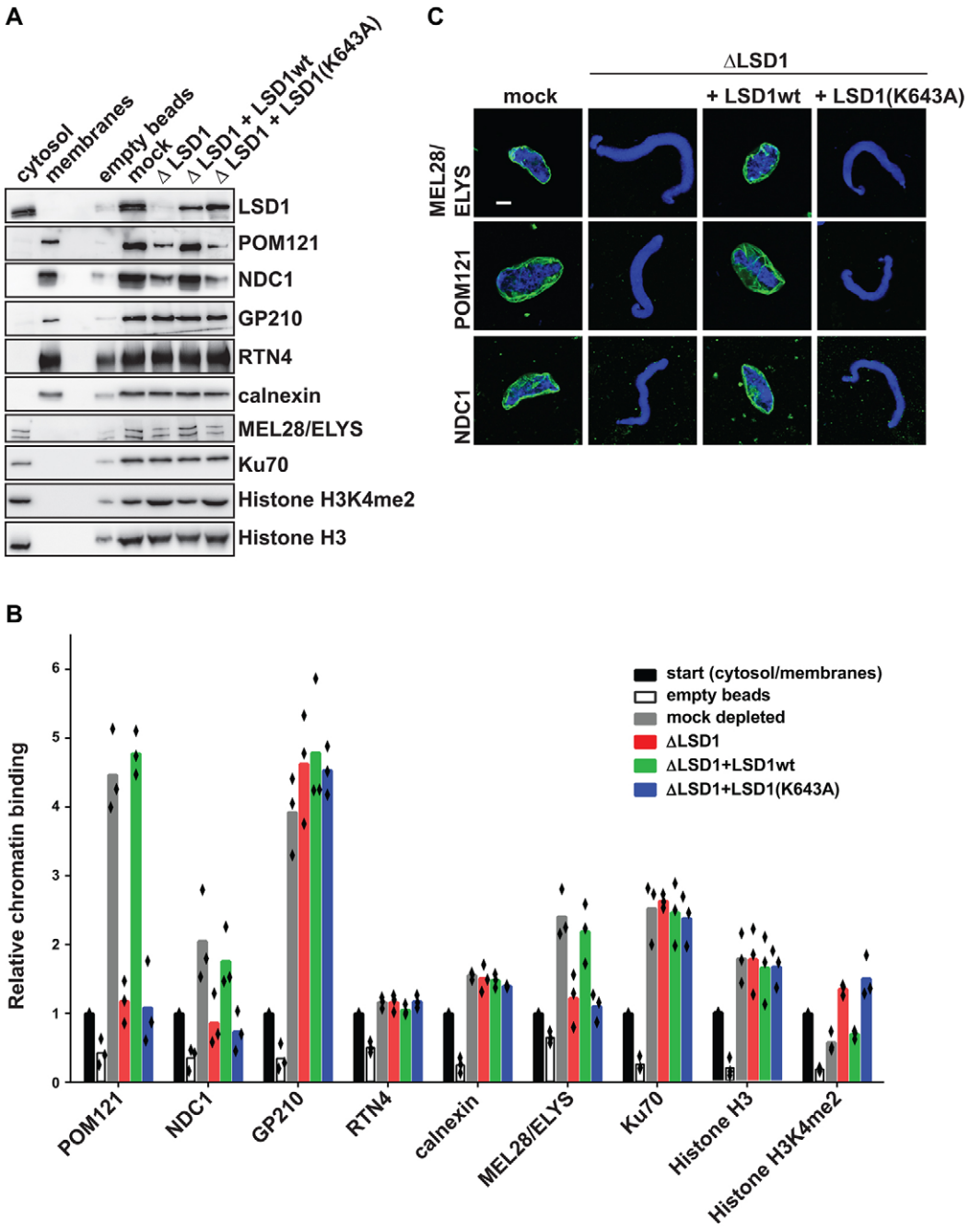

Fig. 6. The recruitment of MEL28, and POM121- and NDC1-containing membrane vesicles to chromatin *in vitro* depends on LSD1. (A) Linearized plasmid DNA immobilized on magnetic beads was chromatinized for 3 h in mock, LSD1-depleted or LSD1-depleted *Xenopus* egg extract cytosol supplemented with either wild-type LSD1 (LSD1wt) or the catalytically inactive LSD1(K643A) mutant, as indicated. After re-isolation, beads were washed and incubated a second time with cytosol treated as before and floatation-purified egg extract membranes. Bead-bound material was re-isolated after 1 h, washed and analysed by western blotting. For comparison, equal amounts (corresponding to the second incubation) of mock-treated extracts and membranes were analysed. Magnetic beads without DNA (empty beads) were used to estimate the background level of binding of extract components to the beads. (B) Quantification of proteins re-isolated with chromatinized DNA beads performed as in A. The mean intensity from three independent experiments normalized to the start material (cytosol or membranes) is plotted. Individual data points are indicated. (C) Nuclei assembled for 120 min in the indicated extracts conditions were fixed and analysed for the presence of MEL28, POM121 and NDC1 (green in overlay) by immunofluorescence and confocal microscopy. Chromatin is stained with DAPI (blue). Scale bar: 5 µm.

Xenopus egg extracts and on chromatinized DNA beads. Consistent with reduced recruitment to DNA beads, nuclei assembled *in vitro* on sperm chromatin in the absence of functional LSD1 lack MEL28, POM121 and NDC1 (Fig. 6C). These data indicate that the efficient recruitment of both MEL28, and POM121- and NDC1-containing nuclear envelope precursor vesicles to chromatin is dependent on LSD1 activity and suggest that LSD1 functions in nuclear assembly by regulating the chromatin-dependent recruitment of nuclear envelope and pore complex proteins at the end of mitosis.

DISCUSSION

The restoration of interphasic nuclear architecture at the end of mitosis requires massive reorganization of the condensed mitotic chromatin and the coordinated reassembly of a functional nuclear envelope. We

Journal of Cell Science (2015) 128, 3466-3477 doi:10.1242/jcs.173013

have found that the catalytic activity of LSD1 plays a crucial role in nuclear formation on post-mitotic chromatin. Interfering with the function of LSD1 either by inhibition or by depletion inhibits cell-free nuclear assembly by blocking chromatin recruitment of MEL28, and POM121- and NDC1-containing membranes. In human cells, reduction of LSD1 by siRNA-mediated depletion severely extends telophase and results in significantly smaller nuclei as well as ectopic NPC formation in the cytoplasm. Our data suggest that in addition to dephosphorylation events and the action of the small GTPase Ran (Hetzer et al., 2002), histone demethylation plays a crucial role in post-mitotic nuclear envelope and pore complex formation.

Mitotic histone modifications are crucial both for marking the interphasic transcriptional state of the chromatin (for a review, see Moazed, 2011; Wang and Higgins, 2013) and for chromosome segregation during anaphase (Kawashima et al., 2010; Yamagishi et al., 2010). The most prominent of these modifications is the phosphorylation of histone H3 at T3, T11, S10 and S28 by the kinases Aurora B and haspin. These marks are removed during mitotic exit by the phosphatase PP1, which is recruited to anaphase chromatin by its targeting cofactor RepoMan (also known as CDCA2) (Trinkle-Mulcahy et al., 2006) and mKI67 (Booth et al., 2014; Takagi et al., 2014). Although it has been recently proposed to be upstream of a histone modification cascade that promotes mitotic chromosome condensation (Wilkins et al., 2014), phosphorylation of histone H3 at S10 is dispensable for chromosome condensation (Hsu et al., 2000; MacCallum et al., 2002) and to date there is no evidence to suggest that the reversal of histone phosphorylation events are specifically required for chromatin decondensation at the end of mitosis (Magalska et al., 2014). Instead, chromatin remodelling downstream of histone dephosphorylation has been linked to nuclear envelope assembly by promoting the recruitment of LBR through heterochromatin protein 1β (HP1β) (Ye et al., 1997; Haraguchi et al., 2000; Fischle et al., 2005) and importin-β-bound nucleoporins through RepoMan (Vagnarelli et al., 2011). The results presented here indicate that demethylation of histone H3 plays a comparable role in the regulation of nuclear reassembly.

Our data suggest that LSD1-mediated demethylation is required for the recruitment of MEL28 and nuclear envelope precursor vesicles, enriched for POM121 and NDC1, to chromatin *in vitro*. In the absence of LSD1, MEL28, and POM121- and NDC1-containing vesicles were not efficiently recruited to chromatinized DNA beads nor were they found on sperm chromatin in 2-h nuclear assembly reactions. These defects were rescued by the addition of recombinant catalytically active LSD1 (Fig. 6). Both MEL28, and POM121- and NDC1-containing vesicles are crucial for NPC assembly (Antonin et al., 2005; Mansfeld et al., 2006; Franz et al., 2007). During mitosis, MEL28 is localized to kinetochores (Rasala et al., 2006). Although it is considered the seeding point for NPC assembly on chromatin (Franz et al., 2007; Gillespie et al., 2007), the precise mechanism governing the redistribution of MEL28 on post-mitotic chromatin is currently unknown. Our data suggest that the proper localization of MEL28 at the end of mitosis depends on changes to chromatin that occur downstream of LSD1 activity. As the recruitment of POM121- and NDC1-containing vesicles to chromatin during nuclear assembly relies on the presence of MEL28 (Rasala et al., 2008), it is likely that the block in nuclear envelope precursor vesicle recruitment we observe occurs, at least partially, upstream of MEL28. However, nuclear envelope precursor vesicles crucial to *in vitro* nuclear assembly, including POM121-containing vesicles, have been found to bind to DNA in the absence of MEL28 (Ulbert et al., 2006). Furthermore, a soluble fragment of POM121 can competitively block nuclear assembly *in vitro* without disrupting the recruitment of MEL28, and in turn the Nup107–Nup160 complex, owing to distinct binding sites on chromatin (Shaulov et al., 2011). Finally, nuclei assembled in the absence of MEL28 form pore-free, albeit closed, nuclear envelopes (Franz et al., 2007), which we did not observe upon LSD1 depletion. Taken together, the nuclear assembly defect we observe in the absence of LSD1 activity is most likely the result of a block in the recruitment of multiple factors that interact independently with chromatin in the early stages of mitotic exit.

Reduction of LSD1 by RNAi significantly extended telophase in HeLa cells. The interphasic nuclei were significantly smaller and we observed a reduction in the total number of NPCs assembled at the nuclear envelope. Because NPC density was not affected by the loss of LSD1 (Fig. 4D), we cannot be certain whether the smaller LSD1-depleted nuclei are specifically defective for NPC formation or rather for nuclear envelope membrane expansion. However, substantial annulate lamellae formation, which is ectopic NPC assembly in the cytoplasm, was also found in LSD1-knockdown cells. Annulate lamellae are typically observed when interfering with NPC re-assembly at the end of mitosis, for example upon MEL28 depletion (Walther et al., 2003b; Franz et al., 2007), suggesting that LSD1 activity is upstream of NPC assembly on chromatin. The relatively modest effect on nuclear envelope assembly in cells could be explained by a lower efficiency of LSD1 depletion compared to the *in vitro* experiments. Although we observed a similar phenotype upon chemical blockade of LSD1 activity (supplementary material Fig. S4A–C), these experiments are difficult to interpret because of predominant cell mortality at the effective concentrations. Alternatively, the role of LSD1-mediated demethylation in post-mitotic nuclear assembly might be partially redundant in HeLa cells. Chemical blockade of LSD1 activity has been found to preferentially inhibit the growth of pluripotent cell types in culture but to have very little impact on the growth rate of HeLa cells (Wang et al., 2011).

The *in vitro* assays employed in our study allowed us to separately query the role of LSD1 in chromatin decondensation and nuclear envelope assembly, events that occur simultaneously in cells. Sperm-chromatin-specific decondensation, an event that occurs immediately after fertilization due to the nucleoplasmin-dependent exchange of sperm protamines for maternal histones (Philpott et al., 1991), was not hindered in LSD1-depleted extracts (Fig. 5A). In uninhibited extracts, decondensed sperm chromatin is the substrate for the assembly of a closed nuclear envelope containing NPCs. Once a functional envelope has formed, the import of nuclear proteins leads to an increase in nuclear volume, a process that is also referred to as nuclear swelling or expansion, or secondary decondensation (Philpott et al., 1991; Wright, 1999). A loss of LSD1 activity, either upon immuno-depletion or after chemical inhibition, blocked nuclear envelope and pore complex formation on the sperm chromatin. In the absence of nuclear envelope formation and the establishment of nuclear import, secondary decondensation could not occur and thus the nuclei assembled appeared small and condensed (Figs 1 and 2). Nevertheless, this should be not misinterpreted as a defect in chromatin decondensation. Similarly, blocking LSD1 activity did not significantly impair the decondensation of mitotic chromatin clusters from HeLa cells in the absence of membranes (Fig. 5B; supplementary material Fig. S4D, top panel). Upon addition of membranes, extracts in which LSD1 activity was removed or blocked gave rise to strikingly smaller nuclei compared to relevant controls (Fig. 5C; supplementary material Fig. S4D, bottom panels).

Journal of Cell Science (2015) 128, 3466-3477 doi:10.1242/jcs.173013

This size discrepancy can be attributed to a loss of secondary decondensation in the absence of a closed and functional nuclear envelope when LSD1 activity is blocked. Our data therefore indicate that chromatin decondensation per se is not dependent on LSD1. Nonetheless, loss of LSD1 activity resulted in smaller nuclei in both our membrane-free decondensation assay (Fig. 5B; supplementary material Fig. S4D) and in HeLa cells (Fig. 4A; supplementary material Fig. S3C and Fig. S4C), suggesting that LSD1 plays a role in reestablishing interphasic chromatin organization at the end of mitosis. Considering its impact on nuclear envelope formation, we postulate that LSD1 is required to generate post-mitotic chromatin that is competent for proper nuclear envelope and NPC assembly.

LSD1 is a nuclear amine oxidase that catalyses the FAD-dependent demethylation of histone H3 at lysine residues 4 and 9 (Shi et al., 2004, 2005; Forneris et al., 2005). It acts mainly as a transcriptional repressor (Shi et al., 2004, 2005; Lee et al., 2005) by demethylating H3K4me2, a mark of active transcription (reviewed in Black et al., 2012). However, it has also been found to demethylate repressive H3K9me2 marks and activate the ligand-dependent transcription of androgen-receptor-responsive genes (Metzger et al., 2005; Wissmann et al., 2007). Importantly, demethylation of histone H3 by LSD1 is locus specific, although the mechanistic details governing this specificity are currently unknown. Consistent with its repressive role, LSD1 has been implicated in heterochromatin formation and maintenance in *Drosophila* and *S. pombe* (Lan et al., 2007; Rudolph et al., 2007).

In the context of mitotic exit, it is not clear how LSD1-dependent demethylation primes chromatin for nuclear envelope assembly and this will be an interesting avenue for future research. Because the catalytic activity of LSD1, and not simply its presence on the chromatin, was required for cell-free nuclear assembly (Fig. 2), it is unlikely that LSD1 itself acts as a scaffold for the recruitment of nuclear envelope proteins at the end of mitosis. Instead, LSD1-mediated demethylation might result in an accumulation of specific histone marks that facilitate the recruitment and assembly of envelope components. Indeed, we observed a twofold increase in dimethylated H3K4 upon LSD1 depletion or re-addition of the catalytically inactive mutant on chromatin beads (Fig. 6A,B). However, the contribution of other histone modifications such as methylated H3K9, another LSD1 target, should not be excluded. It is equally possible that in modulating chromatin organization downstream of histone H3 demethylation, either globally or at the chromatin surface, LSD1 promotes a state of chromatin that is competent for nuclear envelope assembly. Finally, LSD1 has been found to demethylate other chromatin-associated proteins including p53 and DNMT1 (Huang et al., 2007; Wang et al., 2009) and it is certainly possible that its role in nuclear envelope assembly is due to demethylation of non-histone substrates.

LSD1 was previously found to localize to the mitotic spindle and to function in chromosome segregation in dividing HeLa cells (Lv et al., 2010). In our live-cell imaging experiments, we observed a tendency towards extended metaphase in LSD1-depleted cells (supplementary material Fig. S3B,G), which could be indicative of spindle-related defects in chromosome alignment. However, we did not observe a significant increase in the number of lagging chromosomes or chromosome bridges in the siRNA-treated cells (data not shown). We found that LSD1 was excluded from chromatin starting at prometaphase and re-associated with chromatin during telophase, concomitant with mAB414 staining and, presumably, nuclear envelope formation but prior to abscission (supplementary material Fig. S2). A similar dissociation of LSD1 from mitotic chromatin has also been observed in mouse embryonic stem cells (Nair et al., 2012). LSD1 is phosphorylated during mitosis (Lv et al., 2010), and it is possible that this phosphorylation controls its association with chromatin. Alternatively, dynamic histone modifications could be responsible for the cell-cycle-dependent localization of LSD1. For example, phosphorylation of histone H3 at serine 10 blocks the binding of LSD1 to a synthetic H3 peptide *in vitro* (Forneris et al., 2005).

The mitotic-dependent dissociation of LSD1 from chromatin modulates rapid gene expression changes in embryonic stem cells (Nair et al., 2012). LSD1 has also been found to maintain both the undifferentiated state and proliferative capacity of pluripotent cells, which express relatively high levels of LSD1 (Sun et al., 2010; Adamo et al., 2011; Yang et al., 2011; Nair et al., 2012). Here, we have identified a new transcription-independent role for LSD1 in the reestablishment of nuclear architecture following mitotic cell division. Whether the capacity for LSD1 to support nuclear envelope formation on post-mitotic chromatin plays a role in cancer, particularly in cancer stem cells where its expression is frequently mis-regulated (reviewed in Amente et al., 2013), remains a question for future research.

MATERIALS AND METHODS

Antibodies and chemicals

Commercial antibodies against the following proteins were used for immunofluorescence in HeLa cells: LSD1 (Abcam, ab17721), α-tubulin (Sigma, T6199), Nup62 (BD Biosciences, 610498), Nup153 (Abcam, SA1, ab96462), Nup88 (BD Biosciences, 611896), Lamin A (Abcam, ab26300), Lamin B2 [EPR9701(B), Abcam, ab151735], Lamin B receptor (Epitomics, 1398-1) and emerin (Sigma, HPA000609). The human MEL28 (Franz et al., 2007) and POM121 (Mansfeld et al., 2006) antibodies were kind gifts from Iain Mattaj (EMBL Heidelberg, Germany) and Ulrike Kutay (ETH Zurich, Switzerland), respectively. mAB414 (Covance, MMS-120R) was used for immunofluorescence in HeLa cells and on *in vitro* assembled nuclei. With the exception of the mAB414 (used to detect Nup62), Ku70 (H3H10, Abcam, ab3114) and CoREST (Millipore, 07-455) antibodies, which were employed for western blotting, antibodies raised against *Xenopus* proteins were employed in immunoblotting and immunofluorescence in assays based on *Xenopus* egg extract. Antibodies against *Xenopus laevis* GP210 (Antonin et al., 2005), NDC1 (Mansfeld et al., 2006), POM121 and RTN4 (Vollmer et al., 2015) have been described previously. For the anti-MEL28 antibody, a construct comprising amino acids 2290–2408 was expressed from a pET28a vector and used for antibody production in rabbits. The same was done for calnexin, using a construct comprising amino acids 516–606. The *Xenopus* anti-LSD1 antibody was generated in rabbits using full-length LSD1 expressed from a pET28a vector and used at 1:1000 as serum for western blotting both in *Xenopus* egg and HeLa cell extracts and 1:100 for immunofluorescence on nuclei assembled *in vitro*. For affinity purification of the antiserum in order to generate affinity resins for depletion experiments (see below) recombinant LSD1 was coupled to Affigel 10 (Biorad).

The LSD1 inhibitors Pargyline-HCL (Sigma), 2PCPA-H_2SO_4 (BPS Bioscience) and S2101 (Calbiochem) were diluted in water and stored at −20°C prior to use. DiIC18 and secondary antibodies (Alexa-Fluor-488-conjugated goat anti-rabbit-IgG and Cy3-conjugated goat anti-mouse-IgG antibodies) were obtained from Invitrogen.

Protein expression and purification

The construct for *Xenopus laevis* LSD1 (GenBank accession number KR078281) was generated from synthetic DNA optimized for codon usage in *E. coli* (Geneart). The K643A mutant was generated by mutagenesis using the QuikChange site-directed mutagenesis kit (Agilent). Sequences were cloned into a modified pET28a vector containing an N-terminal yeast SUMO solubility tag followed by a TEV cleavage site. Proteins were expressed in *E. coli* and purified by Ni-affinity chromatography. His_6- and SUMO-tags were cleaved using tabacco etch virus (TEV) protease and proteins were concentrated using VIVASPIN columns (Sartorius) prior to

further purification by size exclusion chromatography (Superdex 200 10/300, GE healthcare) in sucrose buffer (250 mM sucrose, 50 mM KCl, 10 mM Hepes-KOH, 2.5 mM $MgCl_2$).

Cell-free nuclear assembly

Nuclear assemblies and immunofluorescence, including the preparation of high-speed interphasic extracts from *Xenopus laevis* eggs, generation of sperm heads and production of floated labelled and unlabelled membranes were performed as described in detail previously (Eisenhardt et al., 2014). Affinity resins used in depletion experiments were generated by crosslinking either purified unspecific rabbit IgG or affinity purified LSD1 IgG to protein-A–sepharose using 10 mM dimethyl pimelimidate (Thermo Scientific). LSD1 was immunodepleted by incubating the resin with egg cytosol in a ratio of 1:1 and rotating at 4°C for 25 min. Unbound cytosol was used immediately. Fluorescence images were acquired using a confocal microscope [FV1000; Olympus; equipped with a photomultiplier (model R7862; Hamamatsu)] using 405-, 488- and 559-nm laser lines and a 60× NA 1.35 oil immersion objective lens.

Cell-free chromatin decondensation

Isolation of mitotic clusters from HeLa cells, preparation of low-speed interphasic egg extracts and chromatin decondensation reactions were performed as described in detail previously (Magalska et al., 2014). Immunodepletion of LSD1 for chromatin decondensation was performed as for nuclear assembly reactions (above). Chromatin decondensation was quantified from confocal images of DAPI-stained nuclei based on two key parameters described previously (Magalska et al., 2014): roughness of the chromatin boundary (perimeter^2/area) and chromatin heterogeneity (the relative internal area occupied by prominent structures, which were recognized using the Fiji StructureJ plugin http://www.imagescience.org/meijering/). Smoothness and homogeneity were defined as the differences from the maximal roughness and maximal relative area, respectively. A maximum of 20% was adopted for the fully decondensed state in both analyses. The fully condensed state was set to zero.

For sperm DNA decondensation, 20 µl of *Xenopus laevis* egg extract was incubated with 0.3 µl sperm heads (3000 sperm heads per µl) for 10 min. Samples were fixed with 4% paraformaldehyde and 0.5% glutaraldehyde on ice, stained with DAPI and analysed on a Axiovert 200 M fluorescence wide-field microscope (Zeiss). Images for both decondensation assays were acquired using a confocal microscope [FV1000; Olympus; equipped with a photomultiplier (model R7862; Hamamatsu)] using 405- and 559-nm laser lines and a 60× NA 1.35 oil immersion objective lens.

Cell culture experiments

HeLa cells were maintained in Dulbecco's modified Eagle's medium (DMEM) supplemented with 2 mM L-glutamine, 10% fetal bovine serum (FBS) and 500 units/ml penicillin-streptomycin (all from Gibco). HeLa cells stably expressing H2B–mCherry (generated as described in Schmitz et al., 2010) were maintained in DMEM additionally supplemented with 0.5 µg/ml puromycin (Gibco). The H2B–mCherry and tubulin–EGFP cell line (Held et al., 2010) was a kind gift from Daniel Gerlich (IMBA, Vienna) and was maintained in DMEM additionally supplemented with 0.5 µg/ml puromycin (Gibco) and 500 µg/ml G-418 (Geneticin; Life Technologies). The following siRNA oligonucleotides were employed in knockdown experiments: siLSD1-1 (AOF2_2), 5′-ACATCTTACCTTAGTCATCAA-3′, siLSD1-2 (AOF2-6), 5′-AGGCCTAGACATTAAACTGAA-3′, and AllStars negative control siRNA (all from Qiagen). Additionally, the following PP2A oligonucleotides were routinely used as a pool mixed 1:1:1 (Schmitz et al., 2010): 5′-GACCAGGATGTGGACGTCAAA-3′, 5′-CCAGGAUGUGGA-CGUCAAATT-3′ and 5′-UUUGACGUCCACAUCCUGGTC-3′ (Qiagen) (Schmitz et al., 2010). Reverse transfections of 20 nM siRNA were carried out in HeLa cell suspensions using Lipofectamine RNAiMAX (Invitrogen) according to the manufacturer's instructions.

HeLa cells were processed for immunofluorescence by fixation with 4% paraformaldehyde (Sigma) in phosphate-buffered saline (PBS) on ice for 10 min prior to permeabilization with 2% Triton X-100 in blocking buffer (3% bovine serum albumine and 0.1% Triton X-100 in PBS). Where indicated, cells were permeabilized prior to fixation with 0.1% Triton-X 100 in a 60 mM PIPES, 20 mM HEPES, 10 mM EGTA, 4 mM $MgSO_4$ buffer (pH 7). Immunofluorescence staining was performed as described previously (Eisenhardt et al., 2014). Images were acquired using a confocal microscope (FV1000; Olympus), 405-, 488- and 559-nm laser lines, and a 60× NA 1.35 oil immersion objective lens. For Nup localization, the photomultiplier (model R7862; Hamamatsu) was employed. The 488-nm laser line and a GaAsP detector were employed to image NPCs for quantification. NPCs labelled with mAB414 were counted for a given surface area from maximum intensity projections comprising five 0.25-µm-spaced optical *z*-sections of the nuclear surface using the Fiji 3D Object Counter (http://fiji.sc/3D_Objects_Counter). The total nuclear volume was measured from the DAPI signal of 0.5 µm optical *z*-sections traversing the entire nucleus using the surpass volume function in IMARIS X64 7.6.3.

For live imaging experiments, HeLa cells expressing H2B–mCherry or both H2B–mCherry and α-tubulin–EGFP were transfected with siRNA oligonucleotides and seeded in eight-well µ-slide chambers (Ibidi). Starting at ~30 h post-transfection, cells were imaged using a Plan-Apochromat 10× NA 0.45 objective and a 561-nm diode laser on a LSM 5 live confocal microscope (Zeiss) equipped with a heating and CO_2 incubation system (Ibidi). ZEN software (Zeiss) was used to acquire images from five 7.5-µm-spaced optical *z*-sections at various *xy* positions every 3 min. Single position *.ome files were generated from the maximum intensity projections in ZEN and converted into image sequences with Fiji software. Segmentation, annotation, classification and tracking of cells progressing through mitosis were performed using the Cecog analyser (http://www.cellcognition.org/software/cecoganalyzer) based on the CellCognition platform (Held et al., 2010).

Chromatin recruitment assay

Coupling of genomic DNA in a linearized plasmid to magnetic M-280 Streptavidin beads (Invitrogen) was as described previously (Ulbert et al., 2006). Once coupled, DNA beads were blocked with 1% lipid-free bovine serum albumin in coupling buffer (2.5% polyvinylalcohol, 1 M NaCl, 50 mM Tris-HCl pH 8.0, 2 mM EDTA), rotating overnight at 4°C. DNA was chromatinized by incubation with high-speed interphasic *Xenopus* egg cytosol (DNA beads:cytosol=1:2.5), shaking at 350 rpm for 3 h at 20°C. Beads were washed once with sucrose buffer and tested for protein recruitment by further incubation with egg cytosol and 10× floated membranes [i.e. tenfold more concentrated than described previously (Eisenhardt et al., 2014)] purified from *Xenopus* eggs (DNA beads:cytosol:membranes=1:0.5:1), shaking at 350 rpm for 1 h at 20°C. After three washes with sucrose buffer, DNA beads were resuspended in Laemmli sample buffer and boiled. Supernatants were subjected to SDS-PAGE and transferred onto nitrocellulose for immunoblotting. Signal intensities were quantified using the Fusion Capt advance software.

Acknowledgements

We thank C. Liebig (Light Microscopy Facility of the MPI for Developmental Biology) for supporting image acquisition and analysis, Alexander Blässle for help with the generation and maintenance of the scripts used to automate the analysis of chromatin decondensation in various assay systems, and Adriana Magalska for helpful discussions.

Competing interests

The authors declare no competing or financial interests.

Author contributions

A.S. and W.A. designed and performed experiments and wrote the manuscript. D.M.-A. performed the live-cell experiments in H2B–mCherry and α-tubulin–EGFP cells and generally supported live-cell experiments and their analysis. B.V. expressed and purified recombinant LSD1. P.D.M. supported the preparation of *Xenopus* egg extracts.

Funding

This work was supported by core funding of the Max Planck Society; and the European Research Council (ERC) [grant number 309528 CHROMDECON to W.A.].

Supplementary material

Supplementary material available online at http://jcs.biologists.org/lookup/suppl/doi:10.1242/jcs.173013/-/DC1

References

Adamo, A., Sesé, B., Boue, S., Castaño, J., Paramonov, I., Barrero, M. J. and Belmonte, J. C. I. (2011). LSD1 regulates the balance between self-renewal and differentiation in human embryonic stem cells. *Nat. Cell Biol.* **13**, 652-660.

Amente, S., Lania, L. and Majello, B. (2013). The histone LSD1 demethylase in stemness and cancer transcription programs. *Biochim. Biophys. Acta* **1829**, 981-986.

Anderson, D. J., Vargas, J. D., Hsiao, J. P. and Hetzer, M. W. (2009). Recruitment of functionally distinct membrane proteins to chromatin mediates nuclear envelope formation in vivo. *J. Cell Biol.* **186**, 183-191.

Antonin, W., Franz, C., Haselmann, U., Antony, C. and Mattaj, I. W. (2005). The integral membrane nucleoporin pom121 functionally links nuclear pore complex assembly and nuclear envelope formation. *Mol. Cell* **17**, 83-92.

Black, J. C., Van Rechem, C. and Whetstine, J. R. (2012). Histone lysine methylation dynamics: establishment, regulation, and biological impact. *Mol. Cell* **48**, 491-507.

Bodoor, K., Shaikh, S., Salina, D., Raharjo, W. H., Bastos, R., Lohka, M. and Burke, B. (1999). Sequential recruitment of NPC proteins to the nuclear periphery at the end of mitosis. *J. Cell Sci.* **112**, 2253-2264.

Booth, D. G., Takagi, M., Sanchez-Pulido, L., Petfalski, E., Vargiu, G., Samejima, K., Imamoto, N., Ponting, C. P., Tollervey, D., Earnshaw, W. C. et al. (2014). Ki-67 is a PP1-interacting protein that organises the mitotic chromosome periphery. *eLife* **3**, e01641.

Daigle, N., Beaudouin, J., Hartnell, L., Imreh, G., Hallberg, E., Lippincott-Schwartz, J. and Ellenberg, J. (2001). Nuclear pore complexes form immobile networks and have a very low turnover in live mammalian cells. *J. Cell Biol.* **154**, 71-84.

Davis, L. I. and Blobel, G. (1986). Identification and characterization of a nuclear pore complex protein. *Cell* **45**, 699-709.

Dultz, E., Zanin, E., Wurzenberger, C., Braun, M., Rabut, G., Sironi, L. and Ellenberg, J. (2008). Systematic kinetic analysis of mitotic dis- and reassembly of the nuclear pore in living cells. *J. Cell Biol.* **180**, 857-865.

Eisenhardt, N., Schooley, A. and Antonin, W. (2014). Xenopus in vitro assays to analyze the function of transmembrane nucleoporins and targeting of inner nuclear membrane proteins. *Methods Cell Biol.* **122**, 193-218.

Fischle, W., Tseng, B. S., Dormann, H. L., Ueberheide, B. M., Garcia, B. A., Shabanowitz, J., Hunt, D. F., Funabiki, H. and Allis, C. D. (2005). Regulation of HP1–chromatin binding by histone H3 methylation and phosphorylation. *Nature* **438**, 1116-1122.

Foisner, R. and Gerace, L. (1993). Integral membrane proteins of the nuclear envelope interact with lamins and chromosomes, and binding is modulated by mitotic phosphorylation. *Cell* **73**, 1267-1279.

Forneris, F., Binda, C., Vanoni, M. A., Mattevi, A. and Battaglioli, E. (2005). Histone demethylation catalysed by LSD1 is a flavin-dependent oxidative process. *FEBS Lett.* **579**, 2203-2207.

Franz, C., Walczak, R., Yavuz, S., Santarella, R., Gentzel, M., Askjaer, P., Galy, V., Hetzer, M., Mattaj, I. W. and Antonin, W. (2007). MEL-28/ELYS is required for the recruitment of nucleoporins to chromatin and postmitotic nuclear pore complex assembly. *EMBO Rep.* **8**, 165-172.

Gant, T. M. and Wilson, K. L. (1997). Nuclear assembly. *Annu. Rev. Cell Dev. Biol.* **13**, 669-695.

Gillespie, P. J., Khoudoli, G. A., Stewart, G., Swedlow, J. R. and Blow, J. J. (2007). ELYS/MEL-28 chromatin association coordinates nuclear pore complex assembly and replication licensing. *Curr. Biol.* **17**, 1657-1662.

Guizetti, J., Schermelleh, L., Mantler, J., Maar, S., Poser, I., Leonhardt, H., Muller-Reichert, T. and Gerlich, D. W. (2011). Cortical constriction during abscission involves helices of ESCRT-III-dependent filaments. *Science* **331**, 1616-1620.

Güttinger, S., Laurell, E. and Kutay, U. (2009). Orchestrating nuclear envelope disassembly and reassembly during mitosis. *Nat. Rev. Mol. Cell Biol.* **10**, 178-191.

Haraguchi, T., Koujin, T., Hayakawa, T., Kaneda, T., Tsutsumi, C., Imamoto, N., Akazawa, C., Sukegawa, J., Yoneda, Y. and Hiraoka, Y. (2000). Live fluorescence imaging reveals early recruitment of emerin, LBR, RanBP2, and Nup153 to reforming functional nuclear envelopes. *J. Cell Sci.* **113**, 779-794.

Harel, A., Orjalo, A. V., Vincent, T., Lachish-Zalait, A., Vasu, S., Shah, S., Zimmerman, E., Elbaum, M. and Forbes, D. J. (2003). Removal of a single pore subcomplex results in vertebrate nuclei devoid of nuclear pores. *Mol. Cell* **11**, 853-864.

Hase, M. E. and Cordes, V. C. (2003). Direct interaction with nup153 mediates binding of Tpr to the periphery of the nuclear pore complex. *Mol. Biol. Cell* **14**, 1923-1940.

Heald, R. and McKeon, F. (1990). Mutations of phosphorylation sites in lamin A that prevent nuclear lamina disassembly in mitosis. *Cell* **61**, 579-589.

Heald, R., Tournebize, R., Blank, T., Sandaltzopoulos, R., Becker, P., Hyman, A. and Karsenti, E. (1996). Self-organization of microtubules into bipolar spindles around artificial chromosomes in Xenopus egg extracts. *Nature* **382**, 420-425.

Held, M., Schmitz, M. H. A., Fischer, B., Walter, T., Neumann, B., Olma, M. H., Peter, M., Ellenberg, J. and Gerlich, D. W. (2010). CellCognition: time-resolved phenotype annotation in high-throughput live cell imaging. *Nat. Methods* **7**, 747-754.

Hetzer, M., Gruss, O. J. and Mattaj, I. W. (2002). The Ran GTPase as a marker of chromosome position in spindle formation and nuclear envelope assembly. *Nat. Cell Biol.* **4**, E177-E184.

Hsu, J.-Y., Sun, Z.-W., Li, X., Reuben, M., Tatchell, K., Bishop, D. K., Grushcow, J. M., Brame, C. J., Caldwell, J. A., Hunt, D. F. et al. (2000). Mitotic phosphorylation of histone H3 is governed by Ipl1/aurora kinase and Glc7/PP1 phosphatase in budding yeast and nematodes. *Cell* **102**, 279-291.

Huang, J., Sengupta, R., Espejo, A. B., Lee, M. G., Dorsey, J. A., Richter, M., Opravil, S., Shiekhattar, R., Bedford, M. T., Jenuwein, T. et al. (2007). p53 is regulated by the lysine demethylase LSD1. *Nature* **449**, 105-108.

Ito, H., Koyama, Y., Takano, M., Ishii, K., Maeno, M., Furukawa, K. and Horigome, T. (2007). Nuclear envelope precursor vesicle targeting to chromatin is stimulated by protein phosphatase 1 in Xenopus egg extracts. *Exp. Cell Res.* **313**, 1897-1910.

Kawashima, S. A., Yamagishi, Y., Honda, T., Ishiguro, K.-i. and Watanabe, Y. (2010). Phosphorylation of H2A by Bub1 prevents chromosomal instability through localizing shugoshin. *Science* **327**, 172-177.

Kessel, R. G. (1992). Annulate lamellae: a last frontier in cellular organelles. *Int. Rev. Cytol.* **133**, 43-120.

Lan, F., Zaratiegui, M., Villén, J., Vaughn, M. W., Verdel, A., Huarte, M., Shi, Y., Gygi, S. P., Moazed, D., Martienssen, R. A. et al. (2007). S. pombe LSD1 homologs regulate heterochromatin propagation and euchromatic gene transcription. *Mol. Cell* **26**, 89-101.

Laurell, E., Beck, K., Krupina, K., Theerthagiri, G., Bodenmiller, B., Horvath, P., Aebersold, R., Antonin, W. and Kutay, U. (2011). Phosphorylation of Nup98 by multiple kinases is crucial for NPC disassembly during mitotic entry. *Cell* **144**, 539-550.

Lee, M. G., Wynder, C., Cooch, N. and Shiekhattar, R. (2005). An essential role for CoREST in nucleosomal histone 3 lysine 4 demethylation. *Nature* **437**, 432-435.

Lv, S., Bu, W., Jiao, H., Liu, B., Zhu, L., Zhao, H., Liao, J., Li, J. and Xu, X. (2010). LSD1 is required for chromosome segregation during mitosis. *Eur. J. Cell Biol.* **89**, 557-563.

MacCallum, D. E., Losada, A., Kobayashi, R. and Hirano, T. (2002). ISWI remodeling complexes in Xenopus egg extracts: identification as major chromosomal components that are regulated by INCENP-aurora B. *Mol. Biol. Cell* **13**, 25-39.

Magalska, A., Schellhaus, A. K., Moreno-Andrés, D., Zanini, F., Schooley, A., Sachdev, R., Schwarz, H., Madlung, J. and Antonin, W. (2014). RuvB-like ATPases function in chromatin decondensation at the end of mitosis. *Dev. Cell* **31**, 305-318.

Mansfeld, J., Güttinger, S., Hawryluk-Gara, L. A., Panté, N., Mall, M., Galy, V., Haselmann, U., Mühlhäusser, P., Wozniak, R. W., Mattaj, I. W. et al. (2006). The conserved transmembrane nucleoporin NDC1 is required for nuclear pore complex assembly in vertebrate cells. *Mol. Cell* **22**, 93-103.

Metzger, E., Wissmann, M., Yin, N., Müller, J. M., Schneider, R., Peters, A. H. F. M., Günther, T., Buettner, R. and Schüle, R. (2005). LSD1 demethylates repressive histone marks to promote androgen-receptor-dependent transcription. *Nature* **437**, 436-439.

Mitchell, J. M., Mansfeld, J., Capitanio, J., Kutay, U. and Wozniak, R. W. (2010). Pom121 links two essential subcomplexes of the nuclear pore complex core to the membrane. *J. Cell Biol.* **191**, 505-521.

Moazed, D. (2011). Mechanisms for the inheritance of chromatin states. *Cell* **146**, 510-518.

Nair, V. D., Ge, Y., Balasubramaniyan, N., Kim, J., Okawa, Y., Chikina, M., Troyanskaya, O. and Sealfon, S. C. (2012). Involvement of histone demethylase LSD1 in short-time-scale gene expression changes during cell cycle progression in embryonic stem cells. *Mol. Cell. Biol.* **32**, 4861-4876.

Peter, M., Nakagawa, J., Dorée, M., Labbé, J. C. and Nigg, E. A. (1990). In vitro disassembly of the nuclear lamina and M phase-specific phosphorylation of lamins by cdc2 kinase. *Cell* **61**, 591-602.

Pfaller, R., Smythe, C. and Newport, J. W. (1991). Assembly/disassembly of the nuclear envelope membrane: cell cycle-dependent binding of nuclear membrane vesicles to chromatin in vitro. *Cell* **65**, 209-217.

Philpott, A. and Leno, G. H. (1992). Nucleoplasmin remodels sperm chromatin in Xenopus egg extracts. *Cell* **69**, 759-767.

Philpott, A., Leno, G. H. and Laskey, R. A. (1991). Sperm decondensation in Xenopus egg cytoplasm is mediated by nucleoplasmin. *Cell* **65**, 569-578.

Pyrpasopoulou, A., Meier, J., Maison, C., Simos, G. and Georgatos, S. D. (1996). The lamin B receptor (LBR) provides essential chromatin docking sites at the nuclear envelope. *EMBO J.* **15**, 7108-7119.

Rasala, B. A., Orjalo, A. V., Shen, Z., Briggs, S. and Forbes, D. J. (2006). ELYS is a dual nucleoporin/kinetochore protein required for nuclear pore assembly and proper cell division. *Proc. Natl. Acad. Sci. USA* **103**, 17801-17806.

Rasala, B. A., Ramos, C., Harel, A. and Forbes, D. J. (2008). Capture of AT-rich chromatin by ELYS recruits POM121 and NDC1 to initiate nuclear pore assembly. *Mol. Biol. Cell* **19**, 3982-3996.

Rotem, A., Gruber, R., Shorer, H., Shaulov, L., Klein, E. and Harel, A. (2009). Importin beta regulates the seeding of chromatin with initiation sites for nuclear pore assembly. *Mol. Biol. Cell* **20**, 4031-4042.

Rudolph, T., Yonezawa, M., Lein, S., Heidrich, K., Kubicek, S., Schäfer, C., Phalke, S., Walther, M., Schmidt, A., Jenuwein, T. et al. (2007). Heterochromatin formation in Drosophila is initiated through active removal of H3K4 methylation by the LSD1 homolog SU(VAR)3-3. *Mol. Cell* **26**, 103-115.

Sachdev, R., Sieverding, C., Flotenmeyer, M. and Antonin, W. (2012). The C-terminal domain of Nup93 is essential for assembly of the structural backbone of nuclear pore complexes. *Mol. Biol. Cell* **23**, 740-749.

Schmitz, M. H. A. and Gerlich, D. W. (2009). Automated live microscopy to study mitotic gene function in fluorescent reporter cell lines. *Methods Mol. Biol.* **545**, 113-134.

Schmitz, M. H. A., Held, M., Janssens, V., Hutchins, J. R. A., Hudecz, O., Ivanova, E., Goris, J., Trinkle-Mulcahy, L., Lamond, A. I., Poser, I. et al. (2010). Live-cell imaging RNAi screen identifies PP2A–B55alpha and importin-beta1 as key mitotic exit regulators in human cells. *Nat. Cell Biol.* **12**, 886-893.

Schooley, A., Vollmer, B. and Antonin, W. (2012). Building a nuclear envelope at the end of mitosis: coordinating membrane reorganization, nuclear pore complex assembly, and chromatin de-condensation. *Chromosoma* **121**, 539-554.

Shaulov, L., Gruber, R., Cohen, I. and Harel, A. (2011). A dominant-negative form of POM121 binds chromatin and disrupts the two separate modes of nuclear pore assembly. *J. Cell Sci.* **124**, 3822-3834.

Shi, Y., Lan, F., Matson, C., Mulligan, P., Whetstine, J. R., Cole, P. A., Casero, R. A. and Shi, Y. (2004). Histone demethylation mediated by the nuclear amine oxidase homolog LSD1. *Cell* **119**, 941-953.

Shi, Y.-J., Matson, C., Lan, F., Iwase, S., Baba, T. and Shi, Y. (2005). Regulation of LSD1 histone demethylase activity by its associated factors. *Mol. Cell* **19**, 857-864.

Stavropoulos, P., Blobel, G. and Hoelz, A. (2006). Crystal structure and mechanism of human lysine-specific demethylase-1. *Nat. Struct. Mol. Biol.* **13**, 626-632.

Stavru, F., Hülsmann, B. B., Spang, A., Hartmann, E., Cordes, V. C. and Görlich, D. (2006). NDC1: a crucial membrane-integral nucleoporin of metazoan nuclear pore complexes. *J. Cell Biol.* **173**, 509-519.

Sun, G., Alzayady, K., Stewart, R., Ye, P., Yang, S., Li, W. and Shi, Y. (2010). Histone demethylase LSD1 regulates neural stem cell proliferation. *Mol. Cell. Biol.* **30**, 1997-2005.

Takagi, M., Nishiyama, Y., Taguchi, A. and Imamoto, N. (2014). Ki67 antigen contributes to the timely accumulation of protein phosphatase 1gamma on anaphase chromosomes. *J. Biol. Chem.* **289**, 22877-22887.

Thompson, L. J., Bollen, M. and Fields, A. P. (1997). Identification of protein phosphatase 1 as a mitotic lamin phosphatase. *J. Biol. Chem.* **272**, 29693-29697.

Trinkle-Mulcahy, L., Andersen, J., Lam, Y. W., Moorhead, G., Mann, M. and Lamond, A. I. (2006). Repo-Man recruits PP1 gamma to chromatin and is essential for cell viability. *J. Cell Biol.* **172**, 679-692.

Ulbert, S., Platani, M., Boue, S. and Mattaj, I. W. (2006). Direct membrane protein-DNA interactions required early in nuclear envelope assembly. *J. Cell Biol.* **173**, 469-476.

Vagnarelli, P., Ribeiro, S., Sennels, L., Sanchez-Pulido, L., de Lima Alves, F., Verheyen, T., Kelly, D. A., Ponting, C. P., Rappsilber, J. and Earnshaw, W. C. (2011). Repo-Man coordinates chromosomal reorganization with nuclear envelope reassembly during mitotic exit. *Dev. Cell* **21**, 328-342.

Vollmer, B., Schooley, A., Sachdev, R., Eisenhardt, N., Schneider, A. M., Sieverding, C., Madlung, J., Gerken, U., Macek, B. and Antonin, W. (2012). Dimerization and direct membrane interaction of Nup53 contribute to nuclear pore complex assembly. *EMBO J.* **31**, 4072-4084.

Vollmer, B., Lorenz, M., Moreno-Andrés, D., Bodenhöfer, M., De Magistris, P., Astrinidis, S. A., Schooley, A., Flötenmeyer, M., Leptihn, S. and Antonin, W. (2015). Nup153 recruits the Nup107-160 complex to the inner nuclear membrane for interphasic nuclear pore complex assembly. *Dev. Cell* **33**, 717-728.

Walther, T. C., Askjaer, P., Gentzel, M., Habermann, A., Griffiths, G., Wilm, M., Mattaj, I. W. and Hetzer, M. (2003a). RanGTP mediates nuclear pore complex assembly. *Nature* **424**, 689-694.

Walther, T. C., Alves, A., Pickersgill, H., Loïodice, I., Hetzer, M., Galy, V., Hülsmann, B. B., Köcher, T., Wilm, M., Allen, T. et al. (2003b). The conserved Nup107-160 complex is critical for nuclear pore complex assembly. *Cell* **113**, 195-206.

Wang, F. and Higgins, J. M. G. (2013). Histone modifications and mitosis: countermarks, landmarks, and bookmarks. *Trends Cell Biol.* **23**, 175-184.

Wang, J., Hevi, S., Kurash, J. K., Lei, H., Gay, F., Bajko, J., Su, H., Sun, W., Chang, H., Xu, G. et al. (2009). The lysine demethylase LSD1 (KDM1) is required for maintenance of global DNA methylation. *Nat. Genet.* **41**, 125-129.

Wang, J., Lu, F., Ren, Q., Sun, H., Xu, Z., Lan, R., Liu, Y., Ward, D., Quan, J., Ye, T. et al. (2011). Novel histone demethylase LSD1 inhibitors selectively target cancer cells with pluripotent stem cell properties. *Cancer Res.* **71**, 7238-7249.

Wilkins, B. J., Rall, N. A., Ostwal, Y., Kruitwagen, T., Hiragami-Hamada, K., Winkler, M., Barral, Y., Fischle, W. and Neumann, H. (2014). A cascade of histone modifications induces chromatin condensation in mitosis. *Science* **343**, 77-80.

Wissmann, M., Yin, N., Müller, J. M., Greschik, H., Fodor, B. D., Jenuwein, T., Vogler, C., Schneider, R., Günther, T., Buettner, R. et al. (2007). Cooperative demethylation by JMJD2C and LSD1 promotes androgen receptor-dependent gene expression. *Nat. Cell Biol.* **9**, 347-353.

Wright, S. J. (1999). Sperm nuclear activation during fertilization. *Curr. Top. Dev. Biol.* **46**, 133-178.

Wurzenberger, C. and Gerlich, D. W. (2011). Phosphatases: providing safe passage through mitotic exit. *Nat. Rev. Mol. Cell Biol.* **12**, 469-482.

Yamagishi, Y., Honda, T., Tanno, Y. and Watanabe, Y. (2010). Two histone marks establish the inner centromere and chromosome bi-orientation. *Science* **330**, 239-243.

Yang, P., Wang, Y., Chen, J., Li, H., Kang, L., Zhang, Y., Chen, S., Zhu, B. and Gao, S. (2011). RCOR2 is a subunit of the LSD1 complex that regulates ESC property and substitutes for SOX2 in reprogramming somatic cells to pluripotency. *Stem Cells* **29**, 791-801.

Yavuz, S., Santarella-Mellwig, R., Koch, B., Jaedicke, A., Mattaj, I. W. and Antonin, W. (2010). NLS-mediated NPC functions of the nucleoporin Pom121. *FEBS Lett.* **584**, 3292-3298.

Ye, Q., Callebaut, I., Pezhman, A., Courvalin, J.-C. and Worman, H. J. (1997). Domain-specific interactions of human HP1-type chromodomain proteins and inner nuclear membrane protein LBR. *J. Biol. Chem.* **272**, 14983-14989.

Supplementary figures

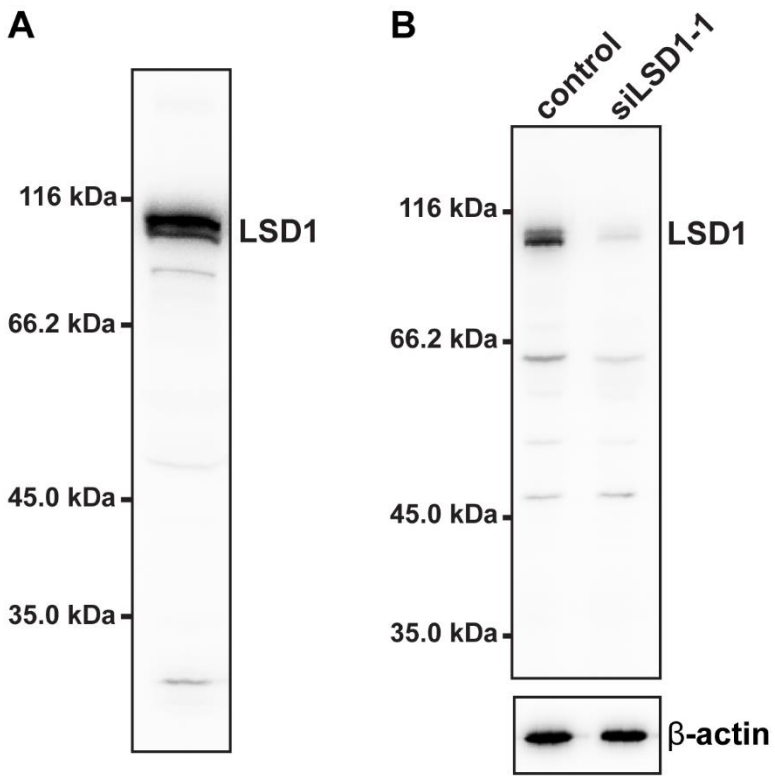

Fig. S1. Characterisation of a new *Xenopus laevis* LSD1 antibody

Antiserum generated in rabbits against the full length *Xenopus laevis* LSD1 protein was tested for specificity in immunoblots of lysates from *Xenopus* egg extracts (A) or HeLa cells (B) subjected to SDS-PAGE. Note the strong reduction of the human LSD1 signal upon RNAi mediated LSD1 downregulation.

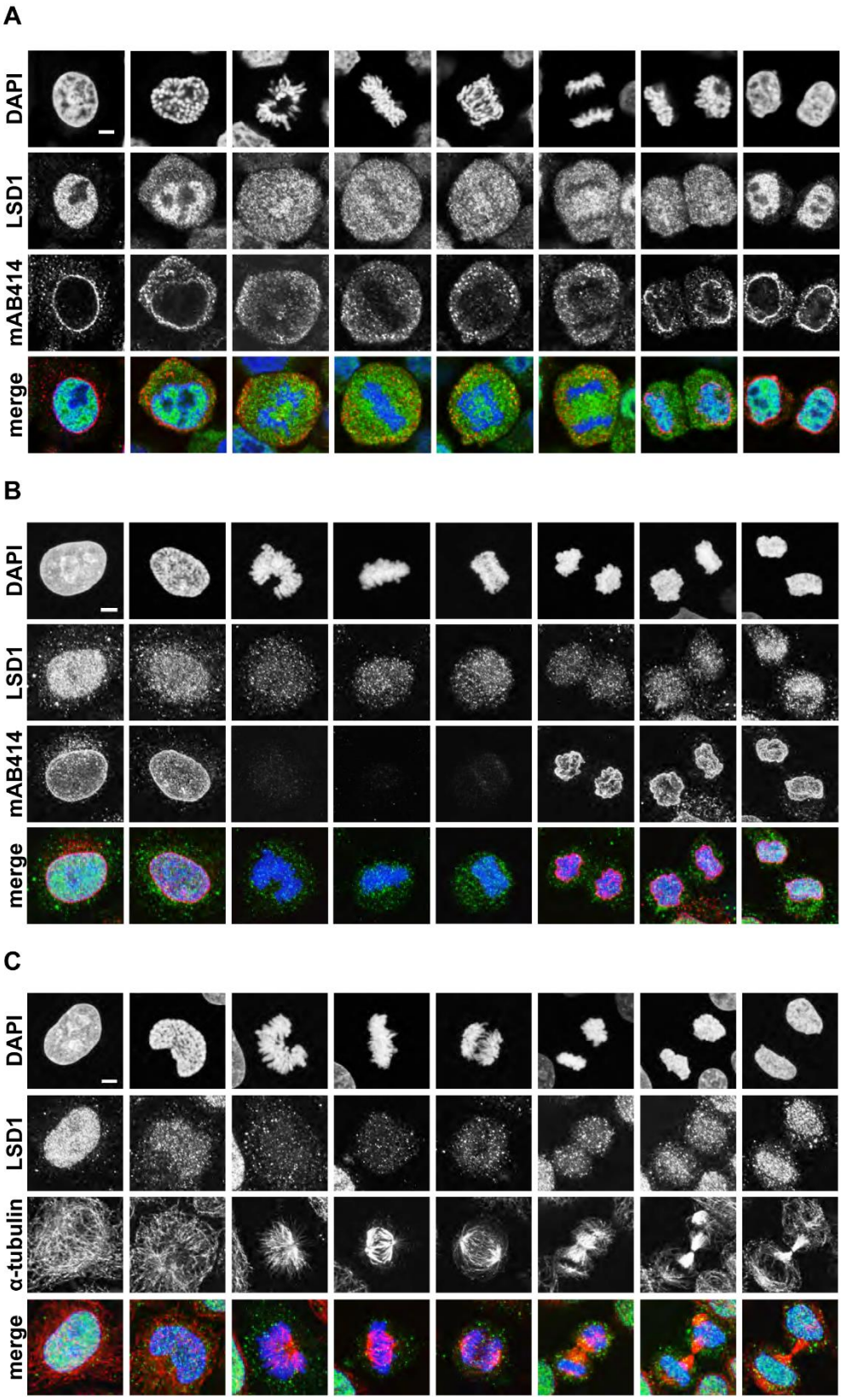

Fig. S2. LSD1 localisation in HeLa cells

(A) The cell cycle-dependent localization of LSD1 in unsynchronised HeLa cells was analyzed by immunofluorescence and confocal microscopy. LSD1 (green in overlay) and NPCs (mAB414, red) were immunolabeled and chromatin was stained with DAPI (blue).

(B) LSD1 (green) and NPCs (mAB414, red) immunolabeled in cells permeabilized with 0.1% Triton-X 100 prior to fixation. Chromatin was stained with DAPI (blue). Maximum intensity projections are shown.

(C) LSD1 (green) and α-tubulin (red) were immunolabeled in cells permeabilized with 0.1% Triton-X 100 prior to fixation. Chromatin was stained with DAPI (blue). Maximum intensity projections are shown.

Scale bars: 5 μm

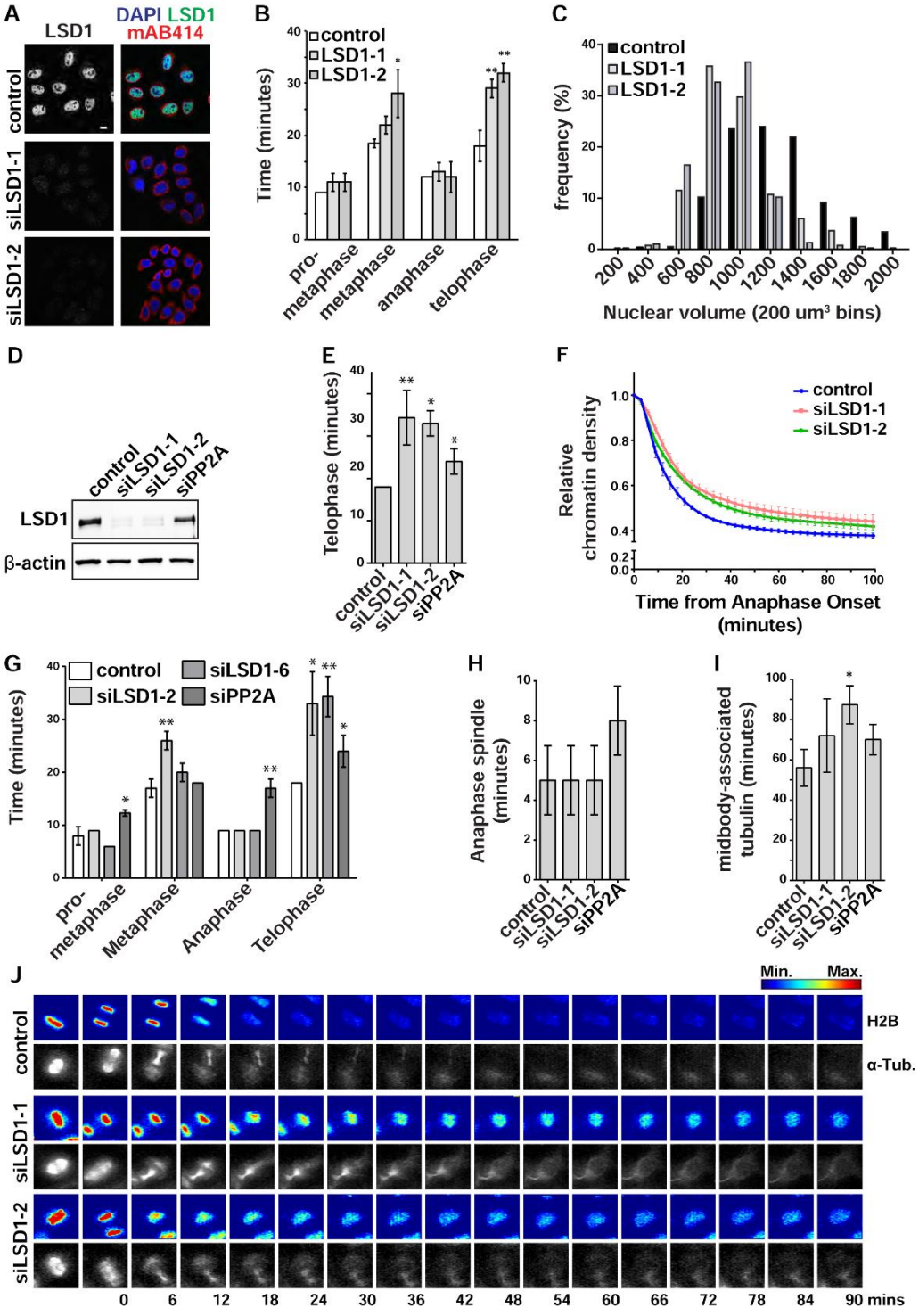

Fig. S3. Further characterization of siRNA mediated downregulation of LSD1 in HeLa cells

(A) HeLa cells transfected with 20 nM control, LSD1-1 or LSD1-2 siRNA oligos were fixed 48h post-transfection and processed for immunofluorescence. LSD1 (top panel, green in overlay) and NPCs (mAB414, red in overlay) were immune-labeled and chromatin was stained with DAPI (blue in overlay). Scale bar: 10 µm

(B) HeLa cells stably expressing H2B-mCherry and transfected with 20 nM siRNA as indicated were subjected to time-lapse microscopy starting 30h post-transfection. Mitotic events were analyzed with CellCognition. The mean of the median time spent in each cell cycle stage indicated is plotted for more than 100 mitotic events per condition in 3 independent experiments. Error bars represent s.d. *P<0.05, Student's t-test.

(C) Quantification of nuclear volume based on DAPI staining in HeLa cells transfected with 20 nM control, LSD1-1 or LSD1-2 siRNA oligos and fixed 48h post-transfection. Nuclear volume measurements from 383 nuclei in 3 independent experiments were pooled for each condition and assigned to 200 μm^3 bins. The nuclear volume frequency for each bin is plotted and the center of each bin is indicated on the x-axis.

(D) Western blot analysis of whole cell lysates from HeLa cells stably expressing H2B-mCherry/α-tubulin-EGFP and transfected with 20 nM control, LSD1-1, LSD1-2, or PP2A siRNA oligos as indicated. Lysates were harvested 48h post-transfection.

(E) HeLa cells stably expressing H2B-mCherry/ α-tubulin-EGFP and transfected with 20 nM siRNA were subjected to time-lapse microscopy starting 30h after transfection. Mitotic events were analyzed with CellCognition. The mean of the median time spent in telophase based on chromatin features is plotted for more than 100 mitotic events per condition in 3 independent experiments. Error bars represent s.d. *P<0.05, **P<0.01, Student's t-test.

(F) The average fluorescence intensity of the H2B-mCherry signal was extracted from the CellCognition data acquired in (B) as an indication of chromatin density. The density was normalized to the first anaphase frame in individual mitotic tracks and the mean relative density for more than 100 mitotic events from three independent experiments is plotted over time. Error bars represent s.d.

(G) HeLa cells stably expressing H2B-mCherry/ α-tubulin-EGFP and transfected with 20 nM siRNA were subjected to time-lapse microscopy starting 30h post-transfection. Mitotic events were analyzed with CellCognition. The mean of the median time spent in each cell cycle stage based on chromatin features is plotted for more than 100 mitotic events per condition in 3 independent experiments. Error bars represent s.d. *P<0.05, **P<0.01, Student's t-test.

(H) HeLa cells stably expressing H2B-mCherry/ α-tubulin-EGFP and transfected with 20 nM siRNA were subjected to time-lapse microscopy starting 30h post-transfection. Mitotic events were analyzed with CellCognition. The mean of the median duration of the anaphase spindle, based on the α-tubulin signal, is plotted for more than 100 mitotic events per condition in 3 independent experiments. Error bars represent s.d.

(I) HeLa cells stably expressing H2B-mCherry/ α-tubulin-EGFP and transfected with 20 nM siRNA were subjected to time-lapse microscopy starting 30h post-transfection. Mitotic events were analyzed with CellCognition. The mean of the median duration of detectable midbody-associated α-tubulin is plotted for more than 100 mitotic events per condition in 3 independent experiments. Error bars represent s.d. *P<0.05, Student's t-test.

(J) HeLa cells stably expressing H2B-mCherry/ α-tubulin-EGFP and transfected with 20 nM siRNA were subjected to time-lapse microscopy starting 30h after transfection. Maximum intensity projections of the mCherry and EGFP signals from five optical z sections are shown. Mitotic tracks are normalized to the first anaphase frame.

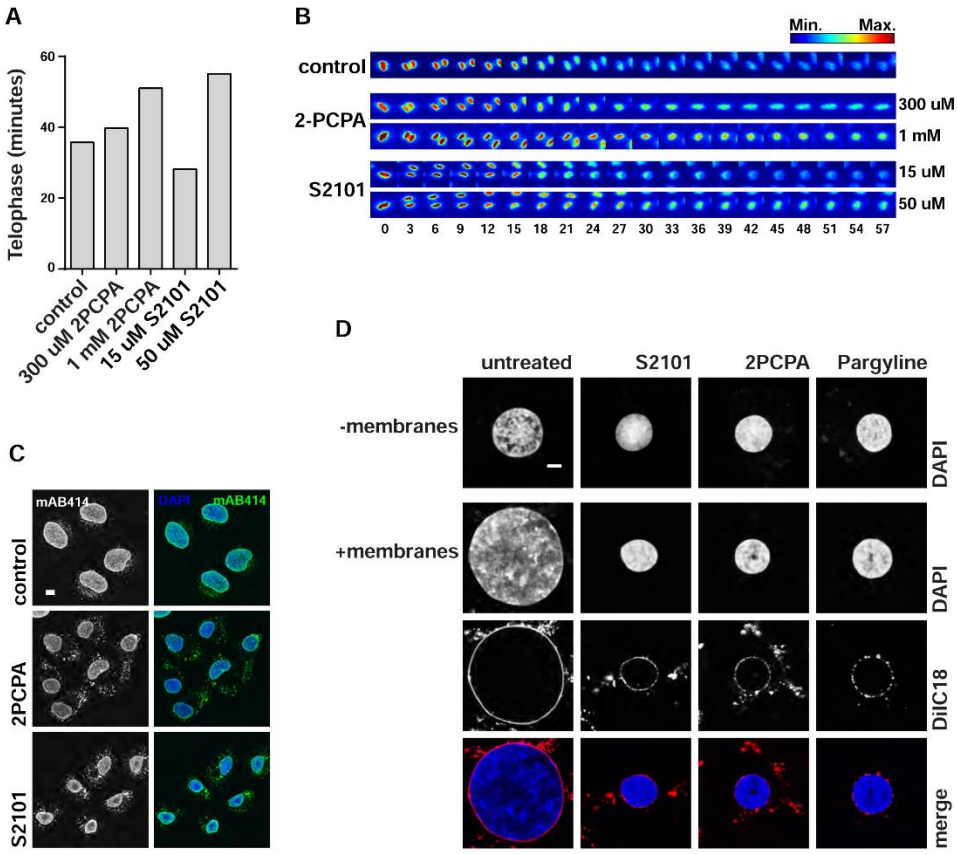

Fig. S4. Chemical inhibition of LSD1 extends the duration of telophase and promotes the formation of annulate lamellae in HeLa cells but does not block membrane-independent chromatin decondensation *in vitro*

(A) HeLa cells stably expressing H2B-mCherry were treated with different concentrations of the LSD1 inhibitors 2-PCPA and S2101 as indicated and immediately subjected to time-lapse microscopy. Mitotic events were analyzed with CellCognition (control: 73 events, 300 µM 2-PCPA: 35 events, 1mM 2-PCPA: 10 events, 15 µM S2101: 62 events, and 50 µM S2101: 22 events). The number of mitotic events analysed was drastically reduced in the presence of LSD1 inhibitors due to cell lethality at the effective concentrations. The median time spent in telophase is plotted and individual data are shown.

(B) HeLa cells stably expressing H2B-mCherry were treated with different concentrations of the LSD1 inhibitors 2-PCPA and S2101 as indicated and immediately subjected to time-lapse microscopy. Representative maximum intensity projections of the mCherry signal from five optical z sections are represented as a heat maps. Mitotic tracks are normalized to the first anaphase frame.

(C) HeLa cells treated with 300 µM 2-PCPA or 15 µM S2101 as indicated for 24h, fixed, and processed for immunofluorescence. NPCs were immuno-labelled using mAB414 (green in overlay) and DNA was stained with DAPI (blue). Maximum intensity projections are shown.

(D) Mitotic chromatin clusters from HeLa cells were incubated with Xenopus egg extracts in the presence or absence of added membranes. Where indicated 5 mM pargyline, 2.5 mM 2PCPA or 0.25 mM S2101 was added to decondensation reactions at t = 0. After 120 min samples were fixed and analyzed by confocal microscopy. Added membranes were pre-labeled with DiIC18 (red in overlay) and chromatin was stained with DAPI (blue in overlay). Scale bar: 5 µm.